

Ground States of the Classical Antiferromagnet on the Pyrochlore Lattice

Matthew F. Lapa^{1,2} and Christopher L. Henley¹

¹*Laboratory of Atomic and Solid State Physics, Cornell University, Ithaca, New York, 14853-2501*

²*Department of Physics, University of Illinois at Urbana-Champaign, 61801-3080*

(Dated: October 26, 2012)

We study the classical ground states of the exchange-coupled Heisenberg antiferromagnet on the Pyrochlore lattice, a non-Bravais lattice made of corner-sharing tetrahedra. In particular, we map out the entire phase diagram for the case of first and second nearest neighbor interactions. In this phase diagram we find *four* complex non-coplanar ground states based on different ordering modes. These are the Cuboctahedral Stack state, a $\langle 111 \rangle$ stacking of Cuboctahedral states, and three families of commensurate spiral: the Kawamura states, constructed from three different combinations of $\{\frac{3}{4}\frac{3}{4}0\}$ modes, the Double-Twist state, also constructed from $\{\frac{3}{4}\frac{3}{4}0\}$ modes, and the Multiply-Modulated Commensurate Spiral state, constructed from $\{\frac{3}{4}\frac{1}{4}\frac{1}{2}\}$ modes. We also briefly look at states involving the two kinds of third nearest neighbor interactions on the Pyrochlore lattice. In this region of parameter space we again find the Cuboctahedral Stack state, and we also find another non-coplanar state in the form of a new kind of Alternating Conic Spiral.

PACS numbers: 75.25.-j, 75.30.Kz, 75.10.Hk, 75.40.Mg

I. INTRODUCTION

This paper concerns the classical ground states of the Heisenberg Hamiltonian on the Pyrochlore lattice, a non-Bravais lattice made of corner-sharing tetrahedra. In this paper we focus our analysis on the case of first and second nearest neighbor interactions J_1 and J_2 , and we briefly mention some results that include the effects of third nearest neighbor interactions J_3 and J'_3 . (Each site on the Pyrochlore lattice has two distinct kinds of third nearest neighbor, at the same separation, yet inequivalent by symmetry – having distinct neighbors at the same distances appears to be universal in non-Bravais lattices.)

An important motivation to work out the phase diagram of magnetic systems is the inverse problem arising from neutron diffraction: not the crystallographic problem of fitting the magnetic structure from the measured Bragg intensities, but rather the physical problem of inferring – in the absence of magnon dispersion relations that would require dynamic neutron scattering – for what possible interactions is the observed structure the ground state. (One motivation for this project was the puzzle presented in Ref. [10] in GeNi_2O_4 , where it was necessary to posit interactions as far as J_4 .)

The other motivation is to facilitate the theorists' pursuit of model systems with unusual properties. For example, whenever frustrated magnets have a large number of degenerate ground states, quantum or thermal fluctuations, or dilution, can select a particular ground state – a form of so-called “ordering due to disorder” [4]. Thus, one interest in our study is to identify parameter combinations on the phase diagram that lead to such degeneracies. This tends to happen along “degenerate phase boundaries” (see Ref. 1, sections II C and VII): their property is that one gets two limiting states depending on which side of the boundary the limit is taken from, yet it is possible to continuously turn one of these into the other within the manifold of degenerate states that exists on the boundary.

Another special property, which we are particularly concerned with in this paper, is inherently *non-coplanar* states. These can produce an *anomalous Hall effect* due to Berry

phases of itinerant electrons [11–14]; they open up possibilities of *multiferroic* behavior [15, 18, 19]; they turn into *chiral* spin liquids if spin order is destroyed; and their symmetry-breaking leads to an order parameter in the form of an $O(3)$ matrix, which allows unusual topological defects (Z_2 vortex and Z_2 domain wall [5]).

The Pyrochlore spin lattice represents many antiferromagnets in any of three well-known crystal structures: the B sites of the spinel structure, one cation sublattice (of the two equivalent ones) in the Pyrochlore structure; or the sublattice of small atoms in the (metallic) Laves phase structure. It is highly degenerate when only the nearest-neighbor interaction is included; in studies where other terms were added that break the degeneracy, surprisingly few of them added farther-neighbor coupling (apart from dipolar spin ice [28]). Instead, anisotropies were added such as local easy planes [29] or Dzyaloshinskii-Moriya anisotropic exchange [30]. Alternatively, lattice distortions were considered [31–34].

In the case of the Pyrochlore, Ref. [24] worked out (in effect) the optimum Luttinger-Tisza modes for general Hamiltonians with J_1 up to J_4 , but limited to $J_3 = J'_3$. The main systematic exploration to date has been of the (J_1, J_2) Pyrochlore [or the (J_1, J_3) case, which is equivalent to the (J_1, J_2) case so long as J_1 is large and antiferromagnetic in sign]. It uncovered a multiple-wavevector, not quite commensurate state with especially soft fluctuations [8, 9, 36, 37] that is not quite fully understood. Another context in which farther neighbor couplings naturally arise is in metallic Pyrochlores, in the form of electron-mediated R.K.K.Y. exchange interactions (that oscillate and decay with separation as a power law).

II. NOTATIONS AND METHODS

In this section we describe the Pyrochlore lattice and we also explain the methods and diagnostics we used to generate and analyze the spin configurations. We present a number of ways of visualizing the Pyrochlore lattice, as certain

ways of thinking about the structure of the Pyrochlore lattice are helpful for understanding certain spin configurations. We also discuss the Iterative Minimization algorithm, our main method of generating spin configurations. Finally we discuss a number of ways of understanding and interpreting the results of the Iterative Minimization simulation, including the Luttinger-Tisza method, numerical Fourier transforms, least square fits and Variational optimization.

A. Pyrochlore Lattice

The Pyrochlore lattice consists of four face-centered cubic (F.C.C.) sublattices, numbered 0, 1, 2 and 3. We take the edge-length of the cubic unit cell of each F.C.C. sublattice to be one. We choose the origins of these four F.C.C. sublattices to be located at $(0, 0, 0)$, $(0, \frac{1}{4}, \frac{1}{4})$, $(\frac{1}{4}, 0, \frac{1}{4})$ and $(\frac{1}{4}, \frac{1}{4}, 0)$, respectively.

Alternately, the Pyrochlore lattice can be viewed as an ABC stacking of triangular and Kagome lattice layers along a $\langle 111 \rangle$ direction in real space as in figure 1.

Our Hamiltonian is

$$\mathcal{H} = -\frac{1}{2} \sum_{i=1}^N \sum_{j \neq i} J_{ij} \mathbf{s}_i \cdot \mathbf{s}_j, \quad (2.1)$$

The \mathbf{s}_i are classical 3-component unit vectors which sit on the sites \mathbf{r}_i of the Pyrochlore lattice. The lattice contains N sites. A positive (negative) J_{ij} represents a ferromagnetic (antiferromagnetic) interaction between the spins \mathbf{s}_i and \mathbf{s}_j . Since the interaction J_{ij} is a function of the displacement vector $\mathbf{R}_{ij} = \mathbf{r}_i - \mathbf{r}_j$ between the spins \mathbf{s}_i and \mathbf{s}_j , we can write $J_{ij} = J(\mathbf{R}_{ij})$.

Each site on the Pyrochlore lattice has six first nearest neighbors, 12 second nearest neighbors and 12 third nearest

neighbors, but the third nearest neighbors come in two kinds, and each site has six of each kind. First nearest neighbors have an interaction J_1 , second nearest neighbors have an interaction J_2 , third nearest neighbors of the first kind have an interaction J_3 and third nearest neighbors of the second kind have an interaction J'_3 . From now on we refer to first nearest neighbors as “ J_1 neighbors”, second nearest neighbors as “ J_2 neighbors”, etc.

The J_1 neighbors of a site can be reached by traveling along one edge of a tetrahedron. The J_2 neighbors of a site can be reached by traveling along two non-collinear edges of two adjacent tetrahedra. The J_3 neighbors of a site can be reached by traveling along two collinear edges of two adjacent tetrahedra. Finally, the J'_3 neighbors of a site can be reached by hopping across a hexagon in the Kagome lattice layers. The two kinds of third nearest neighbors are obviously inequivalent by symmetry since every two J_3 neighbors have a spin lying halfway between them on the line connecting them, while there is no spin lying on the line connecting two J'_3 neighbors.

In this rest of this paper we limit our study to J_1 and J_2 , except that J_3 and J'_3 are used in Section V and Appendix B, and J_3 is mentioned in Section IV C.

B. Luttinger-Tisza Analysis

The Luttinger-Tisza method [3, 6] is a method for finding the ordering wavevector that characterizes the lowest energy state of (2.1) for a given set of interactions J_{ij} . Recall that the goal of any method (analytical or computational) for finding the ground states of (2.1) is to find the set of N spins $\{\mathbf{s}_i\}$ which minimize the total energy subject to the constraint that all of the spins have unit length, i.e. $|\mathbf{s}_i|^2 = 1 \forall i$. The constraint that all of the spins have unit length is often called the *strong constraint*.

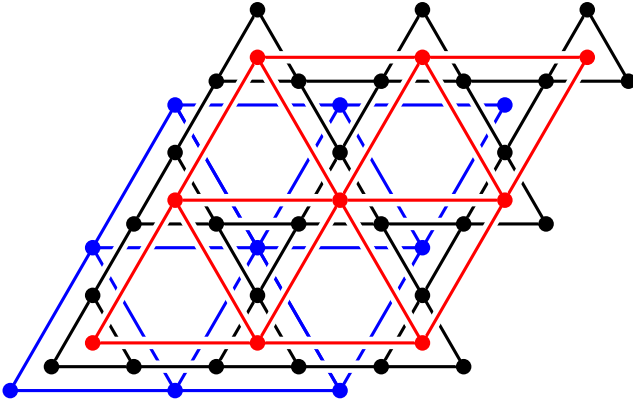
The Luttinger-Tisza method attempts to accomplish this by instead trying to minimize (2.1) subject to what is known as the *weak constraint*,

$$\sum_i |\mathbf{s}_i|^2 = N. \quad (2.2)$$

By formulating the problem in terms of the Fourier Transforms of the spin configuration in each Bravais sublattice, one can obtain a lower bound on the energy of the true ground state. One then searches for a solution to the weak constraint problem which is composed solely of modes related by the symmetry of the underlying Bravais lattice. In an ideal situation we would be able to find a solution to the weak constraint problem that also satisfies the strong constraint, is composed solely of modes related by the symmetry of the underlying Bravais lattice, and has an energy equal to the lower bound. If such a configuration could be found, it would rigorously be the ground state.

To formulate the method we first rewrite equation (2.1) in a way which clearly shows which spins are in which Bravais sublattice. We use the notation $\alpha(i)$ to indicate which Bravais sublattice spin i belongs to, so the possible values for $\alpha(i)$ are 0, 1, 2 and 3 in our case. When it is convenient we will

FIG. 1: The Pyrochlore lattice can be viewed as a stacking of two-dimensional triangular and Kagome lattice layers along a $\langle 111 \rangle$ axis. The picture shows one (black) Kagome lattice layer sandwiched between an upper (red) triangular lattice layer and a lower (blue) triangular lattice layer.



also write $i \in \alpha$ to indicate that spin \mathbf{s}_i is located in the α^{th} Bravais sublattice. From here on we specialize to the case of the Pyrochlore lattice, which has four F.C.C. sublattices. Then we can write

$$J_{ij} \equiv J_{\alpha(i)\beta(j)}(\mathbf{R}_{ij}) \quad (2.3)$$

where $J_{\alpha\beta}(\mathbf{R})$ is the interaction between spins in F.C.C. sublattices α and β that are separated by a vector \mathbf{R} .

Next we define the Fourier Transform of the spin configuration in the α^{th} Bravais sublattice to be

$$\tilde{\mathbf{S}}_\alpha(\mathbf{q}) = \frac{1}{\sqrt{N/4}} \sum_{i \in \alpha} \mathbf{s}_i e^{-i\mathbf{q} \cdot \mathbf{r}_i}, \quad (2.4)$$

where \mathbf{q} is a wavevector in the Brillouin zone of the F.C.C. lattice and $N/4$ is the number of spins in each F.C.C. sublattice. The inverse transform is

$$\mathbf{s}_i = \frac{1}{\sqrt{N/4}} \sum_{\mathbf{q}} e^{i\mathbf{q} \cdot \mathbf{r}_i} \tilde{\mathbf{S}}_{\alpha(i)}(\mathbf{q}). \quad (2.5)$$

Substituting this into (2.3) yields the result

$$\mathcal{H} = - \sum_{\mathbf{q}} \sum_{\alpha, \beta} \tilde{J}^{\alpha\beta}(\mathbf{q}) \tilde{\mathbf{S}}_\alpha(\mathbf{q}) \cdot \tilde{\mathbf{S}}_\beta(-\mathbf{q}). \quad (2.6)$$

The coefficients of the quadratic form (2.6) form a 4×4 matrix $\tilde{\mathcal{J}}(\mathbf{q})$ with matrix elements

$$\tilde{J}_{\alpha\beta}(\mathbf{q}) \equiv \frac{1}{2} \sum_{j \neq i} J_{\alpha(i)\beta(j)}(\mathbf{R}_{ij}) e^{i\mathbf{q} \cdot \mathbf{R}_{ij}}. \quad (2.7)$$

Let $\lambda_\nu(\mathbf{q})$ be the four eigenvalues of this matrix at wavevector \mathbf{q} , each with a normalized eigenvector $u_\alpha^\nu(\mathbf{q})$, where α runs over the four sublattices. These modes, transformed back to the actual lattice as $u_i^\nu \equiv u^\nu(\mathbf{r}_i)$, are exactly analogous to the Bloch wavefunction for the ν band. Express the spin configuration in terms of these eigenmodes:

$$\tilde{\mathbf{S}}_\alpha(\mathbf{q}) = \sum_{\nu} \tilde{\mathbf{w}}_\nu u_\alpha^\nu(\mathbf{q}), \quad (2.8)$$

so the coefficients have three Cartesian components for spin. The total energy is then

$$\mathcal{H} = - \sum_{\mathbf{q}} \sum_{\nu} \lambda_\nu(\mathbf{q}) |\tilde{\mathbf{w}}_\nu(\mathbf{q})|^2. \quad (2.9)$$

Let $\lambda_{max}(\mathbf{q})$ be largest eigenvalue of the matrix $\tilde{\mathcal{J}}(\mathbf{q})$ and let $\mathbf{Q}_{L.T.}$ be a wavevector that maximizes $\lambda_{max}(\mathbf{q})$ (generically there is a star of symmetry-related wavevectors with magnitude $|\mathbf{Q}_{L.T.}|$ that all do this). The quantity $\lambda_{L.T.} \equiv \lambda_{max}(\mathbf{Q}_{L.T.})$ is called the optimal Luttinger-Tisza eigenvalue, and $\mathbf{Q}_{L.T.}$ is the optimal Luttinger-Tisza wavevector. We refer to $\tilde{\mathcal{J}}(\mathbf{Q}_{L.T.})$ as the Luttinger-Tisza matrix.

In Fourier space the weak constraint (2.2) becomes $\sum_{\mathbf{q}, \nu} |\tilde{\mathbf{w}}_\nu(\mathbf{q})|^2 = N$ so the ground state energy manifestly satisfies the inequality

$$\mathcal{H} \geq -N\lambda_{L.T.}. \quad (2.10)$$

A necessary condition for achieving this minimum is that the three components of $\tilde{\mathbf{S}}_\alpha(\mathbf{q})$ be linear combinations of the Luttinger-Tisza eigenmodes $u_\alpha^\nu(\mathbf{Q}_{L.T.})$. The Luttinger-Tisza method works if one can find a normalized spin configuration composed solely of eigenmodes of $\mathbf{Q}_{L.T.}$ (and symmetry-related wavevectors) which also achieves the lower bound on the energy, $-N\lambda_{L.T.}$. On non-Bravais lattices, it is not always possible to construct a normalized state using only Luttinger-Tisza eigenmodes. Many states require admixtures of a set of suboptimal modes in order to achieve normalization [1]. Our experience working with the Pyrochlore lattice confirms that this is true.

The key difficulty with the Luttinger-Tisza method is to ensure $|\mathbf{s}_i| \equiv 1$ for every site, when that is not generally the case for a Luttinger-Tisza eigenmode (expressed in real space, where it appears as a plane wave with a certain weight on each sublattice). On Bravais lattices, that is the case if the eigenmodes are written as complex plane waves $\exp(i\mathbf{Q}_{L.T.} \cdot \mathbf{r})$; from this we can always construct a ground state in the form of a coplanar spiral by using one component for the sine and another for the cosine [3]. Since the optimal Luttinger-Tisza wavevectors typically occur in symmetry-related stars, a non-trivial degeneracy would be possible by taking linear combinations of two modes with different \mathbf{Q} 's from the same star; however, since each mode requires two spin components, that is not possible with physical three-component spins. But whenever $\mathbf{Q}_{L.T.}$ is half of a reciprocal lattice vector (and thus lies on a special point of the Brillouin zone boundary), we have $\exp(i\mathbf{Q}_{L.T.} \cdot \mathbf{r}) = \pm 1$. Thus the plane-wave modes are *real* in this case, and we can combine up to three of them, associated with orthogonal spin directions, to construct continuous families of degenerate classical ground states.

For each set of couplings J_{ij} , we can calculate the optimal Luttinger-Tisza wavevector $\mathbf{Q}_{L.T.}$. This allows us to create a ‘‘Luttinger-Tisza phase diagram’’, showing in what domains of parameter space each kind of L.T. mode is optimal. The L.T. phase diagram tells us the expected wavevector content of the ground state for a given set of couplings, but cannot tell how those modes are combined to construct a normalized state, whether there are multiple degenerate ways to do so, or whether the actual ground state requires admixtures of suboptimal modes for normalization. So although the Luttinger-Tisza phase boundaries typically correspond closely to the real phase boundaries, the true phase diagram often has extra subdivisions that the LT phase diagram lacks, e.g. the three Kawamura states (which all use the same Luttinger-Tisza modes, with admixtures of suboptimal modes).

C. Iterative Minimization method

Following Ref. 1, our main method for finding the ground states of (2.1) is the Iterative Minimization simulation, a numerical approach which starts with a random spin configuration and generates states with progressively lower energy, until the method converges to some (local) energy minimum. Let us first define the local field \mathbf{h}_i to be minus the gradient of (2.1) with respect to the components of spin i (analog of the

force in a mechanical system):

$$\mathbf{h}_i \equiv -\frac{\delta \mathcal{H}}{\delta \mathbf{s}_i} = \sum_{j \neq i} J_{ij} \mathbf{s}_j. \quad (2.11)$$

In any ground state, every spin must be aligned parallel to its local field. (If any spin were not, reorienting it along its local field would immediately lower the energy.)

The method works in the following way. We start with N spins on the Pyrochlore lattice, all pointing in random directions. Next we run a large loop, and on each iteration of the loop we pick N spins at random (one at a time) and reorient them so that they point along their local field.

In our simulations we mostly work on a lattice that is an $L_x \times L_y \times L_z$ block of Pyrochlore lattice unit cells (where L_x , L_y and L_z are integers) with periodic boundary conditions. We also have the capability to use twist boundary conditions, in which spins near a certain boundary of the lattice see their neighbors beyond that boundary twisted by an angle θ about a certain axis in spin space.

Once we have obtained a spin configuration using Iterative Minimization, we try to get a sense of the basic structure of the state using a few simple diagnostics. These are the Site Energy diagnostic, which gives a rough sense of the layout of the spin configuration in real space, the Common-Origin plot, which indicates which directions the spins are pointing in in spin space, and numerical Fourier Transforming, which gives the wavevector content of the state. Finally, we use Least Square fits of the spin configuration to the wavevectors appearing in the numerical Fourier Transform to get an approximate parameterization for the ground state. For simpler states, we can then use the technique of Variational Optimization to determine the idealized values of the parameters appearing in our approximate parameterization of the state. (All of these except the site energy were introduced in Ref. 1.)

1. Site energy diagnostic

We define the site energy of the spin \mathbf{s}_i to be

$$\mathcal{E}_i = -\frac{1}{2} \sum_{j \neq i} J_{ij} \mathbf{s}_i \cdot \mathbf{s}_j. \quad (2.12)$$

The average of this quantity over all the spins in the lattice is the “energy per site” and we denote it by $\bar{\mathcal{E}} \equiv \frac{1}{N} \sum_i \mathcal{E}_i$. The total energy of the system can then be written as $\mathcal{H} = N\bar{\mathcal{E}}$.

We often find that spin configurations break up into sublattices in real space according to the site energy of the spins in those sublattices. Sometimes these sublattices are the familiar four F.C.C. sublattices of the Pyrochlore lattice, as in the Cuboctahedral Stack state (see section V), but sometimes the spin configuration breaks up into a more exotic set of sublattices, as in the Kawamura Sextuplet-q state (see section VI A).

2. Fourier Transforming

Once we have found a spin configuration using Iterative Minimization, we take Fourier Transforms of that spin configuration in each F.C.C. sublattice. Next we compute the Spin Structure Factor in each F.C.C. sublattice to determine which wavevectors the configuration mostly consists of. The Fourier Transform of the spin configuration in the α^{th} F.C.C. sublattice is

$$\tilde{\mathbf{S}}_\alpha(\mathbf{q}) = \frac{1}{\sqrt{N/4}} \sum_{i \in \alpha} \mathbf{s}_i e^{-i\mathbf{q} \cdot \mathbf{r}_i} \quad (2.13)$$

where \mathbf{q} is a wavevector in the Brillouin zone of the F.C.C. lattice and the sum is taken over all spins \mathbf{s}_i in the α^{th} F.C.C. sublattice. In practice we compute these Fourier Transforms one spin component at a time.

We then examine $|\tilde{\mathbf{S}}_\alpha(\mathbf{q})|^2$ for each F.C.C. sublattice (here the square includes a sum over the three Cartesian components from the spins, as well as real/imaginary parts from the Fourier transform.) Sorting these in order of decreasing weight identifies the main wavevectors that characterize the state, which can then be checked against the list of optimal Luttinger-Tisza wavevectors to help determine whether the spin configuration found from Iterative Minimization ought to be a ground state.

3. Common-Origin plot

As in Ref. 1, we use the Common-Origin plot to easily see which directions the spins point in spin space. To construct a Common-Origin plot using a spin configuration determined by Iterative Minimization, we simply plot all the spin vectors with their tails at the origin. This diagnostic lets us easily see which directions the spins point in, but it doesn’t give any information about how the spins are arranged on the lattice.

One can also make Common-Origin plots using only a subset of the entire spin configuration. For example, we might make a Common-Origin plot using only spins in one of the F.C.C. sublattices. To give another example, in cases where the lattice sites break up into sublattices according to site energy, we can make a Common-Origin plot using only spins with a certain site energy. Making Common-Origin plots of subsets of spins like these is often very helpful for finding a symmetrical basis for spin space to rotate the spin configuration into. It is much easier to think of possible idealized forms for a ground state when the numerical spin configuration obtained from Iterative Minimization has been rotated into the most symmetrical basis for spin space.

D. Least Squares Fits and Variational Optimization

Many of the ground states we find in Iterative Minimization simulations are quite complicated, owing to the fact that they contain small contributions from many wavevectors besides

the optimal Luttinger-Tisza wavevectors. In cases like these, it is desirable to obtain an approximate parameterization of the ground state. This approximate parameterization can then be used to obtain a more complete understanding of the state. To find these approximate parameterizations we perform a least squares fit of the numerical spin configuration in each F.C.C. sublattice to sines and cosines of the optimal Luttinger-Tisza wavevectors. If the spin configuration is rotated into a symmetrical basis in spin space, then this method usually yields approximate parameterizations which reveal the main structure of the ground state.

When the least squares fit is simple enough (i.e. it only involves one or two wavevectors), we can idealize the approximate parameterization into a guess for the closed-form parameterization of the ground state. Usually this guess involves a number of unknown parameters (e.g. wavevectors or cone-angles) whose values we compute by analytically solving for the values of these parameters which minimize the energy of the idealized state. This procedure is known as “variational optimization” [1].

When we present parameterizations of spin configurations, we give a formula $\mathbf{S}_\alpha(\mathbf{r})$, which represents the spin configuration as a function of position in the α^{th} F.C.C. sublattice. We usually give the components of $\mathbf{S}_\alpha(\mathbf{r})$ in a Cartesian basis $\{\hat{\mathbf{e}}_1, \hat{\mathbf{e}}_2, \hat{\mathbf{e}}_3\}$ for spin space. Some states, however, take on their simplest form when written in terms of a basis for spin space which rotates as one moves from site to site in real space. It is important to remember that the basis vectors for spin space have no special orientation relative to the crystal lattice, since equation (2.1) is invariant under a uniform rotation of all the spins.

E. Projection of Stacked or Columnar States onto Lower Dimensional Lattices

In this section we discuss a method for analyzing *stacked* and *columnar* states, in which the spin configuration is independent of one or two of the spatial coordinates, respectively, by projecting the lattice and interactions down onto an equivalent one or two-dimensional lattice.

A *stacked* state is one in which there is a certain direction in real space, say $\hat{\mathbf{q}}$, such that within every plane normal to $\hat{\mathbf{q}}$, all the spins have the same direction. Then we can project the three-dimensional lattice down onto an equivalent one-dimensional lattice (as elaborated in Ref. 1, Section V B), in which each spin represents an entire plane of spins from the original three-dimensional lattice. The three-dimensional spin interactions are correspondingly projected to the one-dimensional chain: the interaction J_{ij} between \mathbf{s}_i and another spin \mathbf{s}_j in the chain, is the sum of all interactions between some particular spin that projects to \mathbf{s}_i and *any* spin in the plane that projects to \mathbf{s}_j .

A *columnar* state is a state in which there is a certain direction $\hat{\mathbf{n}}$, such that in any column of sites parallel to $\hat{\mathbf{n}}$, all the spins point in the same direction. In this case, we can project the three-dimensional lattice and its interactions down onto an equivalent two-dimensional lattice, in which each spin repre-

sents an entire line of spins in the original three-dimensional lattice. Similarly to the stacked case, the interaction between two spins \mathbf{s}_i and \mathbf{s}_j in this two-dimensional lattice is equal to the sum of all interactions in three dimensions between one spin in the preimage of \mathbf{s}_i and all spins in the preimage of \mathbf{s}_j .

If the result of an Iterative Minimization simulation is a *stacked* or *columnar* state, then we can make some progress towards understanding that state by projecting the lattice and interactions down onto a lower dimensional lattice. This lower dimensional problem is typically easier to analyze, and in cases where the lower dimensional lattice is a Bravais lattice, we can immediately use the Luttinger-Tisza method to rigorously justify the ground state. If a *stacked* or *columnar* state is the ground state of the three-dimensional lattice, then it must also be the ground state of the lower dimensional lattice (but the converse is not true).

The mapping of stacked states was introduced in Ref. [1] for the study of conic spiral states, which break up into a family of parallel planes such that the spin direction is uniform within each plane. The state can be optimal in three dimensions only if its projection is optimal on the one-dimensional lattice, but the converse is not true. (That is, a state might be optimal on the one-dimensional lattice, but in 3D another state that is not stacked in that way might have an even lower energy.)

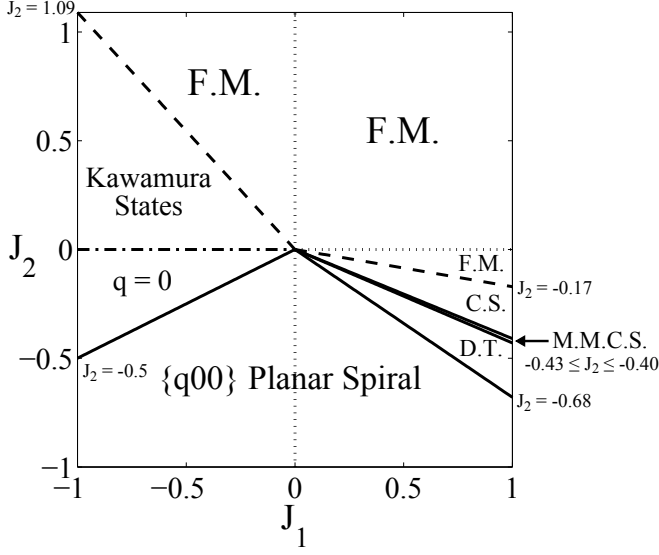
The one-dimensional lattice can have a non-coplanar ground state only if it is non-Bravais lattice, i.e. only if the mapped sites are inequivalent by translation. Thus, it appears that the parallel layers of spins in the three-dimensional lattice must be *unequal*. This happens in the Octahedral lattice of Ref. [1] for (100) layers; in the Pyrochlore lattice the (111) stacking consists of triangular-lattice linking layers, alternating with kagomé-lattice layers that have three times as many spins.

In the case of the Pyrochlore lattice, stacked states in which $\hat{\mathbf{q}}$ is a $\langle 100 \rangle$ direction project onto a one-dimensional Bravais lattice; columnar states in which $\hat{\mathbf{n}}$ is a $\langle 100 \rangle$ direction project onto the two-dimensional non-Bravais lattice known as the Checkerboard lattice [20]. States which are stacked along a $\langle 111 \rangle$ direction project down onto a one-dimensional non-Bravais lattice with a basis of two kinds of site, which are projected respectively from a triangular lattice layer of spins and a Kagome lattice layer of spins. The ground states of (2.1) on this two-site chain lattice, with various couplings, were studied extensively in Ref. 1.

III. OVERVIEW OF RESULTS

In this section we present a brief overview of our results. Most of our work was dedicated to characterizing the ground states of (2.1) for all possible combinations of first and second nearest neighbor interactions, culminating in the J_1 - J_2 phase diagram. We also briefly explored a few ground states that include interactions beyond second nearest neighbors.

FIG. 2: The J_1 - J_2 Phase Diagram for the Pyrochlore Lattice. It shows the regions of the J_1 - J_2 phase diagram in which the Ferromagnetic (F.M.), Kawamura, $\mathbf{q} = \mathbf{0}$, $\{q00\}$ Planar Spiral, Double-Twist (D.T.), Multiply-Modulated Commensurate Spiral (M.M.C.S.) and Cuboctahedral Stack (C.S.) states are found. Solid lines represent first order phase transitions and dashed lines represent second order phase transitions. The dashed-dotted line along the negative J_1 axis indicates that there are a vast number of degenerate ground states along that line and that the Kawamura and $\mathbf{q} = \mathbf{0}$ states are members of that family of degenerate states. We call this a “degenerate” phase transition.



A. The J_1 - J_2 Phase Diagram

The J_1 - J_2 phase diagram is shown in figure 2. The ground states that we find in this region of parameter space are summarized in table I. The two largest regions in the phase diagram are the Ferromagnetic (F.M.) region and the $\{q00\}$ Planar Spiral region. In the region $J_1 > 0$, $J_2 > 0$ the ground state is ferromagnetic (section IV A). This is true even in the case of a pure ferromagnetic J_1 interaction or a pure ferromagnetic J_2 interaction. The reason for this is that the J_1 and J_2 interactions act between spins in different F.C.C. sublattices, so they couple together all of the spins in the lattice. The Ferromagnetic state extends into the $J_1 < 0$, $J_2 > 0$ and $J_1 > 0$, $J_2 < 0$ regions of the J_1 - J_2 phase diagram, although it is quickly destabilized by the antiferromagnetic interactions found in those regions.

The $\{q00\}$ Planar Spiral (section IV E) is a stacked state in which the spins spiral in a plane in spin space as one walks in a particular $\langle 100 \rangle$ direction in the lattice. This state exists in both the $J_1 < 0$, $J_2 < 0$ and $J_1 > 0$, $J_2 < 0$ regions of the J_1 - J_2 phase diagram. In the special case where $J_1 = 0$ and $J_2 < 0$, the $\{q00\}$ Planar Spiral is a 120° spiral in a $\langle 100 \rangle$ direction in the lattice. This special case corresponds to the negative J_2 axis in figure 2, which lies within the region where the $\{q00\}$ Planar Spiral is the ground state.

Ground State	J_1	J_2	NCP? (y/n)	$\mathbf{Q}_{L.T.}$
Ferromagnetic (F.M.)	+, -	+, -	n	(0,0,0)
$J_1 < 0$	-	0	n	Any
$\{q00\}$ Planar Spiral	+, -	-	n	$\{q00\}$
$\mathbf{q} = \mathbf{0}$	-	-	n	(0,0,0)
Cuboctahedral Stack (C.S.)	+	-	y	$\{\frac{1}{2} \frac{1}{2} \frac{1}{2}\}$
Kawamura States	-	+	y	$\{\frac{3}{4} \frac{3}{4} 0\}$
Double-Twist (D.T.)	+	-	y	$\{\frac{3}{4} \frac{3}{4} 0\}$
Multiply-Modulated Commensurate Spiral (M.M.C.S.)	+	-	y	$\{\frac{3}{4} \frac{1}{2} \frac{1}{4}\}$

TABLE I: Summary of the ground states found in the J_1 - J_2 phase diagram. It tells the region of the phase diagram where each state is found, whether or not the state is non-coplanar (NCP), and also gives the optimal Luttinger-Tisza wavevector $\mathbf{Q}_{L.T.}$ for each state.

The next largest region in figure 2 is the region in the $J_1 < 0$, $J_2 > 0$ quadrant where the ground states are the three Kawamura States (section VI); the Sextuplet-q state, the Quadruplet-q state of type 1 and the Quadruplet-q state of type 2. The Fourier Transforms of these three states consist primarily of $\{\frac{3}{4} \frac{3}{4} 0\}$ wavevectors. At $J_1 \approx -1.09J_1$ the Kawamura States transition to the ferromagnetic state.

In the upper part of the $J_1 < 0$, $J_2 < 0$ quadrant of figure 2 the ground state is the $\mathbf{q} = \mathbf{0}$ state (section IV C), in which all spins in the same F.C.C. sublattice are parallel to each other, so that the spins point in only four directions in spin space. These four spin directions also add to zero because of the antiferromagnetic J_1 interaction. At $J_2 = 0.5J_1$ this state transitions to the $\{q00\}$ Planar Spiral state.

Finally, there are three more ground states in the $J_1 > 0$, $J_2 < 0$ quadrant of figure 2. The first of these is the Cuboctahedral Stack (C.S.) state (section V), a non-coplanar state in which the spins point towards the eight corners and 12 edge-midpoints of a cube in spin space. As J_2 is made more negative there is a transition to the Multiply-Modulated Commensurate Spiral (M.M.C.S.) state (section VIII), a non-coplanar state in which the spins perform two different kinds of spirals which are controlled by two distinct wavevectors. Lastly there is the Double-Twist (D.T.) state (section VII), a non-coplanar state in which the spins perform two different kinds of spirals but those two kinds of spirals are controlled by the same kind of wavevector.

We have arranged our discussion of these states roughly in the order of least complicated to most complicated. In the section dealing with the simpler states (section IV) we have grouped together states which are closely related. So, for example, the discussion of the $\mathbf{q} = \mathbf{0}$ state comes directly after the discussion of the ground states of the pure $J_1 < 0$ antiferromagnet, of which it is a special case. The Cuboctahedral Stack state is the most complicated state for which we still have an exact parameterization and energy per site, so our section on this state (section V) can be said to bridge the gap between the less complicated and more complicated states.

B. States with J_3 and J'_3

In our exploration of states involving the third nearest neighbor interactions J_3 and J'_3 , we again found the Cuboctahedral Stack state, and we also found a new kind of Alternating Conic Spiral state. We found that one can also stabilize the Cuboctahedral Stack state with a ferromagnetic J_1 interaction, a ferromagnetic J_3 interaction and an antiferromagnetic J'_3 interaction. We conjecture that the two regions of parameter space in which the Cuboctahedral Stack is the ground state (i.e. this region and the region in the J_1 - J_2 plane) are smoothly connected.

When the magnitude of the antiferromagnetic J'_3 interaction becomes much larger than the magnitudes of the ferromagnetic J_1 and J_3 interactions, we find a new kind of Alternating Conic Spiral state (appendix B). This state is different from the alternating conic spirals discovered in Ref. 1 in the sense that the wavevector which controls the spiraling behavior and the wavevector which controls the alternating behavior are not parallel to each other.

IV. SIMPLE STATES

We start our tour of the phase diagram with the most elementary cases, in that there is only one coupling, and/or there are ground states with the periodicity of the unit cell. All these states are exact Luttinger-Tisza states whose exact energies are known, and in none of these cases is a non-coplanar state forced.

A. Ferromagnetic State

The simplest state we find (and the simplest possible ground state) is the ferromagnetic state, in which every spin points in the same direction. This state is obviously the ground state in the region where J_1 and J_2 are both greater than zero, but we also find it in the region $J_1 < 0$, $J_2 > 0$ when $J_2 \geq -1.09J_1$ and in the region $J_1 > 0$, $J_2 < 0$ when $J_2 \geq \left(-\frac{3}{8} + \frac{\sqrt{6}}{12}\right)J_1$. The energy per site of the ferromagnetic state is

$$\bar{\mathcal{E}} = -3J_1 - 6J_2. \quad (4.1)$$

If the interactions are J_1 , J_3 and J'_3 (section V D), the energy per site of the ferromagnetic state is

$$\bar{\mathcal{E}} = -3J_1 - 3J_3 - 3J'_3. \quad (4.2)$$

We use these expressions for the energy per site of the ferromagnetic state to predict where this state transitions to competing states in the regions $J_1 > 0$, $J_2 < 0$ and $J_1 < 0$, $J_2 > 0$, and also in regions of the phase diagram where J_3 and J'_3 are non-zero.

B. Pure $J_1 < 0$

The ground state of (2.1) in the case of a pure antiferromagnetic first nearest neighbor interaction $J_1 < 0$ is well known to be any state in which the sum of the four spins on each tetrahedron is equal to zero. One can prove this using the Cluster method [7], in which one finds a way to rewrite the Hamiltonian as a sum of disjoint terms: if a state can be exhibited in which each term is separately minimized, this must be a ground state (and all other ground states must have the same property)

Let the tetrahedra in the lattice be indexed by the Greek letter η and let the spin in F.C.C. sublattice α on the η^{th} tetrahedron be $s_{\eta,\alpha}$. Then the pure- J_1 Hamiltonian takes the form

$$\mathcal{H} = -\frac{1}{2}J_1 \sum_{\eta} |\mathbf{L}_{\eta}|^2 + \text{constant}, \quad (4.3)$$

where $\mathbf{L}_{\eta} = \sum_{\alpha=0}^3 s_{\eta,\alpha}$, i.e. the sum of the four spins on the η^{th} tetrahedron.

Eq. (4.3) is a sum over disjoint terms, each of which is minimized by

$$\mathbf{L}_{\eta} = \mathbf{0}. \quad (4.4)$$

Furthermore it is easy to find an example configuration that satisfies condition (4.4) simultaneously on all tetrahedra, so we can rigorously conclude this condition is true for all η in *all* ground states. In any such a state, the site energy is $\mathcal{E}_i = J_1$ for *every* spin, so the energy per site is also

$$\bar{\mathcal{E}} = J_1. \quad (4.5)$$

These states have an extensive degeneracy, meaning the number of parameters needed to specify the spin configuration is proportional to the number of spins in the system. The $\mathbf{q} = \mathbf{0}$ states of Sec. IV C and the Kawamura states of Sec. VI still satisfy the constraint (4.4) so they are specific subsets of the ground states for the pure $J_1 < 0$ case.

C. $\mathbf{q} = \mathbf{0}$ State(s) ($J_1 < 0$ and $J_2 < 0$)

In the region $J_1 < 0$, $\frac{1}{2}J_1 \leq J_2 \leq 0$ we find a state in which all spins in the same F.C.C. sublattice are parallel and the spins from the four F.C.C. sublattices all sum to zero. To be more precise, we have $\mathbf{S}_{\alpha} = \mathbf{n}_{\alpha}$, where the \mathbf{n}_{α} are all constant unit vectors which satisfy

$$\sum_{\alpha=0}^3 \mathbf{n}_{\alpha} = \mathbf{0}. \quad (4.6)$$

We call this state a $\mathbf{q} = \mathbf{0}$ state because the wavevector characterizing the spin configuration in each F.C.C. sublattice is the zero wavevector. The site energy for each spin in this state is $\mathcal{E}_i = J_1 + 2J_2$ so this state has an energy per site equal to

$$\bar{\mathcal{E}} = J_1 + 2J_2. \quad (4.7)$$

For sufficiently small J_2 , at least, the ground state must be a subset of the pure- J_1 ground state manifold of Section IV B, selected by J_2 as a degenerate perturbation. This state is most quickly understood by using the equivalence of a small anti-ferromagnetic (ferromagnetic) J_2 interaction with a small ferromagnetic (antiferromagnetic) J_3 interaction, within that degenerate manifold (see Ref. 8 for a proof of this fact). The reason for this equivalence is the following. The J_2 and J_3 interactions of spin i can be gathered into contributions from six second-neighbor tetrahedra, each of which includes a different J_1 neighbor of spin i . But in view of (4.4) the sum of the two J_2 neighbors, the one J_3 neighbor, and the one J_1 neighbor in each of those tetrahedra is zero, hence the sum of the J_1 , J_2 , and J_3 energies is also zero – but the total J_1 energy is a fixed constant within the degenerate manifold satisfying (4.5).

So, we can trade this problem for that of a small $J_3 > 0$. Since the J_3 bonds connect sites of same F.C.C. sublattice, the J_3 term is optimized when all spins in the same F.C.C. sublattice are parallel (so $\mathbf{q} = \mathbf{0}$ by definition). This is compatible with (4.4): the necessary and sufficient condition is Eq. (4.6), as was claimed.

Thus the $\mathbf{q} = \mathbf{0}$ states form a continuous two-dimensional manifold of degenerate states, inequivalent by rotational symmetry, and parametrized by two angles, θ and ϕ . We can define $\theta \in [0, \pi]$ to be the angle between \mathbf{n}_0 and \mathbf{n}_1 – this must also be the angle between \mathbf{n}_2 and \mathbf{n}_3 , since $|\mathbf{n}_0 + \mathbf{n}_1| = |\mathbf{n}_2 + \mathbf{n}_3|$; then we can take $\phi \in [0, \pi]$ to be the angle between the plane of $(\mathbf{n}_0, \mathbf{n}_1)$ and that of $(\mathbf{n}_2, \mathbf{n}_3)$.

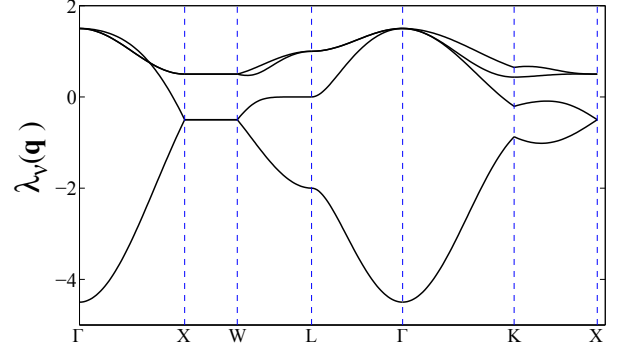
Because the $\mathbf{q} = \mathbf{0}$ family satisfies the constraint (4.6), this state is also a ground state of (2.1) in the case of a pure first nearest neighbor interaction $J_1 < 0$. Evidently, the set of $\mathbf{q} = \mathbf{0}$ states is just a subset of the ground states for the pure $J_1 < 0$ interaction, and these states are selected out by the antiferromagnetic J_2 interaction.

Figure 3 shows the four eigenvalues $\lambda_\nu(\mathbf{q})$ of the matrix $\tilde{J}(\mathbf{q})$ plotted along the $\Gamma \rightarrow X \rightarrow W \rightarrow L \rightarrow \Gamma \rightarrow K \rightarrow X$ route through the Brillouin zone of the F.C.C. lattice for the parameter values $J_1 = -1$, $J_2 = -0.25$. We see that the largest eigenvalue has its maximum at the Γ point $\mathbf{q} = \mathbf{0}$, so the optimal L.T. wavevector is $\mathbf{Q}_{L.T.} = \mathbf{0}$, not only for small J_2 but in a considerable interval. Since we constructed normalized spin states using just these modes, they are rigorously the ground states, and Iterative Minimization simulations confirm this.

D. Pure $J_2 < 0$

Unlike the case of a pure J_3 interaction, in which the Hamiltonian breaks down into uncoupled sublattices, the pure J_2 interaction acts between sublattices, so that every spin is coupled to every other one. In the case of a pure antiferromagnetic second nearest neighbor interaction, we find that the ground state is a 120° planar spiral stacked in a $\langle 100 \rangle$ direction in the lattice. We can get an understanding of this state by *assuming* (based on evidence from Iterative Minimization simulations) that the state is stacked along a $\langle 100 \rangle$ direction and

FIG. 3: The four eigenvalues $\lambda_\nu(\mathbf{q})$ of the matrix $\tilde{J}(\mathbf{q})$ plotted along the $\Gamma \rightarrow X \rightarrow W \rightarrow L \rightarrow \Gamma \rightarrow K \rightarrow X$ route through the the Brillouin zone of the F.C.C. lattice for $J_1 = -1$, $J_2 = -0.25$, where the ground state is the $\mathbf{q} = \mathbf{0}$ state. Recall that $\Gamma = (0, 0, 0)$, $X = 2\pi(1, 0, 0)$, $W = 2\pi(1, \frac{1}{2}, 0)$, $K = 2\pi(\frac{3}{4}, \frac{3}{4}, 0)$ and $L = 2\pi(\frac{1}{2}, \frac{1}{2}, \frac{1}{2})$. The largest eigenvalue of $\tilde{J}(\mathbf{q})$ takes on its maximum value at the Γ point $\mathbf{q} = \mathbf{0}$, confirming that the optimal L.T. wavevector in this region is $\mathbf{Q}_{L.T.} = \mathbf{0}$, as expected.



then projecting the interactions down onto an equivalent one-dimensional lattice. We can then apply the Luttinger-Tisza method [3, 6] to this equivalent one-dimensional lattice. We use the method outlined in subsection II E to determine the effective interactions in the equivalent one-dimensional lattice.

Let us take the stacking to be along the z -direction. The (001) planes of sites with the same spin direction are separated by a distance of $\frac{1}{4}$. A spin has four of its second nearest neighbors in each adjacent plane (separated by a distance $\frac{1}{4}$ in the z direction) and two more second nearest neighbors in planes that are two steps away (i.e. separated by $\frac{1}{2}$ in the z direction). Thus, the equivalent one-dimensional lattice has both first and second neighbor interactions, $j_1 = 4J_2$ and $j_2 = 2J_2 = \frac{1}{2}j_1$. In addition, the one-dimensional lattice is a Bravais lattice, because every site in the same constant- z plane has the same number of second nearest neighbors in the planes above and below it.

The optimal wavevector takes the form $\mathbf{q} = (0, 0, q)$ in the three-dimensional lattice. In the one-dimensional lattice the state will be characterized by a wavenumber q_{1d} . We have $q = q_{1d}/2$ since in the three-dimensional lattice the minimum separation in the z direction between two spins in the same F.C.C. sublattice with the same x and y coordinates is $\frac{1}{2}$, whereas the minimum separation between two spins in the one-dimensional Bravais sublattice is $\frac{1}{4}$. Since the minimum separation in the z direction between two spins in the same sublattice is doubled when going from the one-dimensional lattice to the three-dimensional lattice, the wavevector is halved.

Applying the Luttinger-Tisza method to the one-dimensional chain gives an expression for $\tilde{J}(q_{1d})$, the Fourier transform of the couplings in the one-dimensional

chain:

$$\tilde{J}(q_{1d}) = 4J_2 \left(2 \cos\left(\frac{q_{1d}}{4}\right) + \cos\left(\frac{q_{1d}}{2}\right) \right) \quad (4.8)$$

Maximizing this we find that the optimal (one-dimensional) wavenumber is given by

$$\cos\left(\frac{q_{1d}}{4}\right) = -\frac{1}{2} \quad (4.9)$$

so we have $q_{1d} = \frac{8\pi}{3}$, which means that spins separated by a distance of $\frac{1}{4}$ in the z-direction (first nearest neighbors in the one-dimensional lattice) are rotated 120° from each other. So the ground state is a 120° spiral in the z-direction. This state has the form

$$\mathbf{S}_{1d}(z) = \cos\left(\frac{8\pi}{3}z\right) \hat{\mathbf{e}}_1 + \sin\left(\frac{8\pi}{3}z\right) \hat{\mathbf{e}}_2 \quad (4.10)$$

in the one-dimensional lattice, up to an arbitrary (constant) phase angle. In the three-dimensional lattice we have $q = \frac{4\pi}{3}$, and we can parameterize this same state as

$$\mathbf{S}_{\alpha=0,3}(\mathbf{r}) = \cos\left(\frac{4\pi}{3}z\right) \hat{\mathbf{e}}_1 - \sin\left(\frac{4\pi}{3}z\right) \hat{\mathbf{e}}_2 \quad (4.11a)$$

$$\begin{aligned} \mathbf{S}_{\alpha=1,2}(\mathbf{r}) = & \cos\left(\frac{4\pi}{3}z + \frac{\pi}{3}\right) \hat{\mathbf{e}}_1 \\ & + \sin\left(\frac{4\pi}{3}z + \frac{\pi}{3}\right) \hat{\mathbf{e}}_2 \end{aligned} \quad (4.11b)$$

in the separate F.C.C. sublattices.

The site energy of each spin is given by $\mathcal{E}_i = 3J_2$ so this state has an energy per site

$$\bar{\mathcal{E}} = 3J_2. \quad (4.12)$$

The 120° spiral is just a special case of the more general $\{q00\}$ planar spiral state, discussed in the next subsection (IV E), which involves both J_1 and J_2 interactions.

E. $\{q00\}$ Planar Spiral ($J_2 < 0$ and $J_1 > 0$ or $J_1 < 0$)

In the region $J_1 < 0$, $J_2 \leq \frac{1}{2}J_1$ and also in the region $J_1 > 0$, $J_2 \leq -0.68J_1$, we find a planar spiral state which is stacked in a $\langle 100 \rangle$ direction, which (as in Sec. IV D) we again take along z . This generalized spiral can also be understood by mapping the interactions down onto an equivalent one-dimensional lattice, now with couplings $j_1 = 2J_1 + 4J_2$ and $j_2 = 2J_2$. Applying the Luttinger-Tisza method to this one-dimensional lattice gives

$$\tilde{J}(q_{1d}) = 2j_1 \cos\left(\frac{q_{1d}}{4}\right) + 2j_2 \cos\left(\frac{q_{1d}}{2}\right). \quad (4.13)$$

so the optimal one-dimensional wavenumber is given by

$$\cos\left(\frac{q_{1d}}{4}\right) = -\frac{j_1}{4j_2} = -\frac{J_1 + 2J_2}{4J_2} \quad (4.14)$$

in terms of the interactions in the three-dimensional lattice. The parameterization of this state in the three-dimensional lattice has the same form as equations (4.11a) and (4.11b), but with $\frac{4\pi}{3}$ replaced by the wavenumber q determined from (4.14) and the relation $q = q_{1d}/2$. The site energy for each spin in this state is

$$\mathcal{E}_i = \frac{J_1^2}{4J_2} + 3J_2, \quad (4.15)$$

so $\bar{\mathcal{E}} = \mathcal{E}_i$. In the special case of $J_1 = 0$, we recover the 120° spiral found in the previous section.

Finally, we note that in order for equation (4.14) to have a solution for q_{1d} , we must have $-1 \leq -\frac{J_1 + 2J_2}{4J_2} \leq 1$. Therefore, this state can only exist in the region $J_1 < 0$ when $J_2 \leq \frac{1}{2}J_1$, and it can only exist in the region $J_1 > 0$ when $J_2 \leq -\frac{1}{6}J_1$.

V. CUBOCTAHEDRAL STACK

In the region $J_1 > 0$, $J_2 < 0$ we find a state that we have named the Cuboctahedral Stack because the spins in each Kagome lattice layer perpendicular to a certain $\langle 111 \rangle$ direction in real space are arranged in the Cuboctahedral state found on the Kagome lattice in Ref. 25 and on the Octahedral lattice in Ref. 1. In each of those states the spins point towards the 12 vertices of a cuboctahedron or, equivalently, the 12 edge-midpoints of a cube. If we choose a basis in spin space in which the sides of this cube are perpendicular to $\langle 100 \rangle$ directions, the spins point in the twelve $\langle 110 \rangle$ directions in spin space.

A. Structure of the Cuboctahedral Stack

In the Cuboctahedral Stack state there is a distinguished direction in real space, which is one of the four $\langle 111 \rangle$ directions (we choose $[111]$ for the parameterizations below). In the Kagome lattice layers stacked perpendicular to this direction, the spins point towards the 12 edge-midpoints of a cube. In the triangular lattice layers between the Kagome layers, the spins point towards the eight corners of that same cube.

This state is built out of three of the four $\{\frac{1}{2}\frac{1}{2}\frac{1}{2}\}$ type wavevectors and the fourth unused wavevector points in the stacking direction of the Kagome and triangular lattice layers; it can be written as

$$\mathbf{S}_0 = \frac{1}{\sqrt{3}} \sum_{k=1}^3 \cos(\mathbf{q}_k \cdot \mathbf{r}) \hat{\mathbf{e}}_k \quad (5.1a)$$

$$\mathbf{S}_{\alpha=1,2,3} = \frac{1}{\sqrt{2}} \sum_{k=1, k \neq \alpha}^3 \cos(\mathbf{q}_k \cdot \mathbf{r}) \hat{\mathbf{e}}_k, \quad (5.1b)$$

where the three wavevectors used in this parameterization are $\mathbf{q}_1 = 2\pi(-\frac{1}{2}, \frac{1}{2}, \frac{1}{2})$, $\mathbf{q}_2 = 2\pi(\frac{1}{2}, -\frac{1}{2}, \frac{1}{2})$ and $\mathbf{q}_3 = 2\pi(\frac{1}{2}, \frac{1}{2}, -\frac{1}{2})$.

In this parameterization, the triangular layers consist of the spins in F.C.C. sublattice 0, whose configuration is given by (5.1a), and the Kagome layers consist of the spins in F.C.C. sublattices 1, 2 and 3, whose configurations are given by (5.1b). The site energies for spins in the four F.C.C. sublattices are

$$\mathcal{E}_i^{(0)} = -\sqrt{6}J_1 \quad (5.2a)$$

$$\mathcal{E}_i^{(1,2,3)} = -J_1 \left(1 + \frac{\sqrt{6}}{3} \right), \quad (5.2b)$$

where the superscript indexes the F.C.C. sublattices. The site energy of a spin in a triangular layer is lower than the site energy of a spin in a Kagome layer.

B. Energy per spin in the cuboctahedral stack

The energy per site in this state is then

$$\bar{\mathcal{E}} = -J_1 \left(\frac{3}{4} + \frac{\sqrt{6}}{2} \right). \quad (5.3)$$

Evidently, the J_2 contribution to the energy of this state completely cancels out, so that the total energy depends only on J_1 .

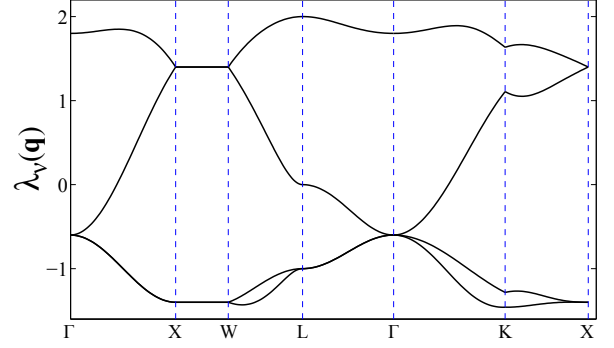
In fact, the lower bound on the energy of this state (from equation (2.10)) is $-2J_1$, so even though the Cuboctahedral Stack is constructed solely from the optimal L.T. wavevectors, it does not achieve the lower bound on the energy. This is related to the fact that only three out of a total of four available symmetry related $\{\frac{1}{2}, \frac{1}{2}, \frac{1}{2}\}$ modes are used to construct this state.

Figure 4 shows the four eigenvalues $\lambda_\nu(\mathbf{q})$ of the matrix $\tilde{J}(\mathbf{q})$ plotted along the $\Gamma \rightarrow X \rightarrow W \rightarrow L \rightarrow \Gamma \rightarrow K \rightarrow X$ route through the Brillouin zone of the F.C.C. lattice for the parameter values $J_1 = 1$, $J_2 = -0.2$. We see that the largest eigenvalue has its maximum at the L point $\mathbf{q} = 2\pi(\frac{1}{2}, \frac{1}{2}, \frac{1}{2})$, confirming that the optimal L.T. wavevector is $\mathbf{Q}_{L.T.} = 2\pi(\frac{1}{2}, \frac{1}{2}, \frac{1}{2})$, as expected from Iterative Minimization simulations.

1. Why energy is independent of J_2

To see why the total energy (5.3) is independent of J_2 , we need to think more about the structure of this state. Of the four spins in every tetrahedron, three of them lie in a Kagome lattice layer and the fourth lies in a triangular lattice layer. Recall that every spin in a triangular lattice layer points in a $\langle 111 \rangle$ direction and every spin in a Kagome lattice layer points in a $\langle 110 \rangle$ direction. To approximately satisfy the ferromagnetic first nearest neighbor interaction, the three spins on a tetrahedron in a Kagome lattice layer will point in three $\langle 110 \rangle$ directions which surround the same corner of a cube in spin space. For example, these spins might point in the $[110]$, $[101]$

FIG. 4: The four eigenvalues $\lambda_\nu(\mathbf{q})$ of the matrix $\tilde{J}(\mathbf{q})$ plotted along the $\Gamma \rightarrow X \rightarrow W \rightarrow L \rightarrow \Gamma \rightarrow K \rightarrow X$ route through the Brillouin zone of the F.C.C. lattice for $J_1 = 1$, $J_2 = -0.2$, where the Cuboctahedral Stack (C.S) state is the ground state. Recall that $\Gamma = (0, 0, 0)$, $X = 2\pi(1, 0, 0)$, $W = 2\pi(1, \frac{1}{2}, 0)$, $K = 2\pi(\frac{3}{4}, \frac{3}{4}, 0)$ and $L = 2\pi(\frac{1}{2}, \frac{1}{2}, \frac{1}{2})$. The largest eigenvalue of $\tilde{J}(\mathbf{q})$ takes on its maximum value at the L point, $\mathbf{q} = 2\pi(\frac{1}{2}, \frac{1}{2}, \frac{1}{2})$, the wavevector which characterizes the Cuboctahedral Stack state.



and $[011]$ directions. Then the dot product between any two of these three spins will be $\frac{1}{2}$. The fourth spin on this tetrahedron, the one which lies in a triangular lattice layer, will then point in the $[111]$ direction, the average of the directions the other three spins point in. The dot product of this fourth spin with any of the other three will then be $\frac{2}{\sqrt{6}} \approx 0.82$, which also favors the ferromagnetic first nearest neighbor interaction.

Because of this structure, the dot product between any spin in a triangular lattice layer (i.e. in F.C.C. sublattice 0) and any of its second nearest neighbors is always zero. The reason for this is that any second nearest neighbor of a spin in a triangular lattice layer will be in a Kagome lattice layer, so it will point in a $\langle 110 \rangle$ direction. Moreover, the $\langle 110 \rangle$ direction it points in will be one which surrounds a corner of the cube in spin space which is adjacent to the corner that the spin in the triangular lattice layer points towards, but this $\langle 110 \rangle$ direction will not point towards the midpoint of the edge that connects these two corners of the cube in spin space. It follows from this that the dot products of a spin in a triangular layer with its second nearest neighbors are all zero.

The dot products between any spin in a Kagome lattice layer and its 12 second nearest neighbors are not all zero but they do add to zero. Of these 12 dot products, four of them are 0 (the dot products with spins in the adjacent triangular layers), four of them are $-\frac{1}{2}$ (the dot products with spins in the same Kagome layer) and four of them are $\frac{1}{2}$ (the dot products with spins in the neighboring Kagome layers which are beyond the adjacent triangular layers).

C. Cuboctahedral stack in the (J_1, J_2) phase diagram

As explained in the last subsection, when we fix J_1 and vary J_2 , the energy of the Cuboctahedral Stack state is unchanging, but the energy of any competing states (whose energy generally does depend on J_2) may cross lower than that of the Cuboctahedral Stack, at which point there will be a phase transition. In particular, comparing Eq. (5.3) to Eq. (4.1), we find that the transition from the ferromagnetic state to the Cuboctahedral Stack should occur at

$$J_2 = \left(-\frac{3}{8} + \frac{\sqrt{6}}{12}\right) J_1 \approx -0.171 J_1, \quad (5.4)$$

and this result is confirmed by simulations. Simulations also show that the Cuboctahedral Stack transitions to the Multiply-Modulated Commensurate Spiral state (section VIII) near $J_2 = -0.40 J_1$.

1. Transition between the Cuboctahedral Stack and ferromagnetic states

Because there are no variable parameters in the parameterization of the Cuboctahedral Stack state, we might expect that the transition between this state and the ferromagnetic state would be of first order. The results of Iterative Minimization simulations show that this is not the case. On the ferromagnetic side of the phase boundary we find a “mixed” state near the transition point whose energy is lower than the energies of both the ferromagnetic and Cuboctahedral Stack states. The Fourier Transform of this mixed state shows peaks at $\mathbf{q} = \mathbf{0}$ as well as at the $\{\frac{1}{2}, \frac{1}{2}, \frac{1}{2}\}$ wavevectors that make up the Cuboctahedral Stack. In spin space the spins are arranged around a cone so that this state does have a net magnetic moment which points along the axis of that cone.

If one looks in detail at the spin directions in the Common-Origin plot, one sees that the spins unfold from the conic axis in four sets of three spins and four sets of two spins, with a set of two spins between every set of three spins. In addition, this configuration is symmetric under a rotation of 90° about the conic axis. It appears that as one approaches the phase boundary from the ferromagnetic side the four sets of three spins become the 12 spins which point in $\langle 110 \rangle$ directions in the Cuboctahedral Stack state, and the four sets of two spins become the eight spins which point in $\langle 111 \rangle$ directions in the Cuboctahedral Stack state.

This evidence suggests that the phase transition between the ferromagnetic and Cuboctahedral Stack states is continuous (of second order) and that the spin configuration near the phase boundary (on the ferromagnetic side) is a configuration which smoothly interpolates between the ferromagnetic and Cuboctahedral Stack states.

D. Cuboctahedral Stack in the J_1, J_3, J'_3 Phase Diagram

The Cuboctahedral Stack state also exists in the J_1, J_3, J'_3 phase diagram for $J_1, J_3 > 0$ and $J'_3 < 0$. This state is

again made up of three of the four $\{\frac{1}{2}, \frac{1}{2}, \frac{1}{2}\}$ type wavevectors, with the fourth unused wavevector pointing in the stacking direction. The parameterization is exactly the same as that presented in equations (5.1a) and (5.1b). The energy per site for the Cuboctahedral Stack state with these three interactions is

$$\bar{\mathcal{E}} = -\left(\frac{3}{4} + \frac{\sqrt{6}}{2}\right) J_1 - J_3 + J'_3. \quad (5.5)$$

This state is expected to transition to the ferromagnetic state, with energy per site (4.2), when

$$J_1 = -\frac{8J_3 + 16J'_3}{9 - 2\sqrt{6}}. \quad (5.6)$$

From our experience with the phase transition between the ferromagnetic and Cuboctahedral Stack states in the J_1 - J_2 phase diagram, we expect that this phase transition will also be of second order.

Previously, we had understood the Cuboctahedral Stack as being the result of competition between a strong ferromagnetic nearest neighbor interaction J_1 and a weak antiferromagnetic second nearest neighbor interaction J_2 . In this case we have no second nearest neighbor interaction, but we do have a ferromagnetic J_3 interaction and an antiferromagnetic J'_3 interaction. In the Cuboctahedral Stack configuration, a spin in a triangular lattice layer has a dot product of $\frac{1}{3}$ with its six J_3 neighbors and a dot product of $-\frac{1}{3}$ with its six J'_3 neighbors. A spin in a Kagome lattice layer has a dot product of 1 with two of its six J_3 neighbors (those in adjacent Kagome lattice layers) and a dot product of 0 with the other four (those in the same Kagome lattice layer) and it also has a dot product of -1 with two of its J'_3 neighbors (those in the same Kagome lattice layer) and 0 with the other four (those in adjacent Kagome lattice layers). In this way the Cuboctahedral Stack state serves as a compromise in which spins have positive (or zero) dot products with their J_3 neighbors and negative (or zero) dot products with their J'_3 neighbors. So the dot product between each pair of spins is either zero or has the sign that goes with the interaction between that pair of spins (e.g. dot products between J_3 neighbors are either zero or positive, which favors the ferromagnetic J_3 interaction).

VI. KAWAMURA STATES

In the region $J_1 < 0$, $0 < J_2 \leq 1.09|J_1|$ of the phase diagram, we encounter a remarkable phase first identified in finite-temperature simulations of Refs. 36 and 37, and further studied in Refs. 8 and 9. This is actually a family of phases dominated by a certain kind of $\{\frac{3}{4}, \frac{3}{4}, 0\}$ ordering mode, which according to the Luttinger-Tisza analysis is optimal in this parameter range. In fact, the exact Luttinger-Tisza wavevector starts out at $\{\frac{3}{4}, \frac{3}{4}, 0\}$ for $J_2 \ll |J_1|$, but it drifts slightly inwards as J_2 is increased, eventually settling at an incommensurate wavevector near $2\pi(0.73, 0.73, 0)$ as J_2 is increased to $J_2 \approx |J_1|$. So the $\{\frac{3}{4}, \frac{3}{4}, 0\}$ wavevectors are only *nearly* optimal in this region of parameter space, although they are very

close to the true L.T. wavevector. By taking linear combinations with multiple symmetry-related modes it is possible to construct three particularly symmetric noncoplanar states [9] that are called the “Sextuplet-q” state, and the “Quadruplet-q states of types 1 and 2”. We have called this whole family the “Kawamura States” after the group which has done the most to elucidate their structure.

The Sextuplet-q state is composed from equal amounts of all six $\{\frac{3}{4}\frac{3}{4}0\}$ wavevectors. The Quadruplet-q state of type 1 is composed from *equal* amounts of four of the $\{\frac{3}{4}\frac{3}{4}0\}$ wavevectors which lie on the points of a cross in reciprocal space. [For example, these might be $2\pi(\frac{3}{4}, \frac{3}{4}, 0)$, $2\pi(\frac{3}{4}, -\frac{3}{4}, 0)$, $2\pi(\frac{3}{4}, 0, \frac{3}{4})$ and $2\pi(\frac{3}{4}, 0, -\frac{3}{4})$.] Finally, the Quadruplet-q state of type 2 is composed of *unequal* amounts of those same four wavevectors. [For example, the largest contribution might be from wavevectors $2\pi(\frac{3}{4}, \frac{3}{4}, 0)$ and $2\pi(\frac{3}{4}, -\frac{3}{4}, 0)$, with a slightly smaller contribution from $2\pi(\frac{3}{4}, 0, \frac{3}{4})$ and $2\pi(\frac{3}{4}, 0, -\frac{3}{4})$.] Furthermore, each of these three states very nearly satisfies the tetrahedron constraint (4.4), so these states are a subset of the pure $J_1 < 0$ anti-ferromagnet of section IV B.

Ref. 9 used mean-field theory to predict the stability of these phases as a function of temperature, concentrating on the particular point $J_2/|J_1| = 0.2$, and found that the cubic Sextuplet-q phase is stable at higher temperatures, while the quadruplet-q kind of state was stable at lower temperatures. [39] In our $T = 0$ study, the three states were nearly degenerate in this region of parameter space. The L.T. phase diagram indicates that the Kawamura states should transition to the ferromagnetic state at $J_2 \approx 1.09|J_1|$. Iterative Minimization simulations confirm that a phase transition does take place at this location and the simulations also seem to show that the transition is of second-order.

Our Iterative Minimization simulations in this region of the J_1 - J_2 phase diagram find these three states, as well as states with slightly higher energies which are also mainly composed of $\{\frac{3}{4}\frac{3}{4}0\}$ wavevectors. Therefore we suspect that the energy landscape in this region of parameter space consists of three local minima representing the three Kawamura states, and that these minima sit in a valley with a gently sloping floor. This would explain why our simulations sometimes don’t find these three local minima and instead settle into states with slightly higher energies.

Even though the three Kawamura states are nearly degenerate in this region of the phase diagram, our Iterative Minimization simulations show that the true ground state is the Sextuplet-q state for $J_2 \ll |J_1|$ at least until $J_2 = 0.1|J_1|$. Somewhere between $J_2 = 0.1|J_1|$ and $J_2 = 0.15|J_1|$ there is a phase transition, and we find that the true ground state for $0.15|J_1| \leq J_2 \leq 1.09|J_1|$ is the Quadruplet-q state of type 2. It appears that the Quadruplet-q state of type 1 is never the true ground state in this region, even though it is always nearly degenerate with the other two Kawamura states.

We have focused our study of the structure of the states in this region almost exclusively on the Kawamura Sextuplet-q state. There are two reasons for this. Firstly, it has the most symmetry in real space and in spin space out of the three Kawamura states. More importantly, it has a slightly lower

Sublattice	\mathcal{E}_i	# of spins
1	-1.1053	192
2	-1.1841	192
3	-1.2103	192
4	-1.2672	64
5	-1.2753	192
6	-1.2902	192

TABLE II: Site energies and number of spins in each sublattice of the Kawamura Sextuplet-q State with $J_1 = -1$, $J_2 = 0.1$, on a lattice of size $4 \times 4 \times 4$.

energy than the other two Kawamura States when $J_2 \ll |J_1|$, suggesting that it is the state selected out of the highly degenerate manifold of pure- J_1 ground states by an infinitesimal ferromagnetic J_2 interaction.

A. Structure of Kawamura Sextuplet-q State

The Kawamura Sextuplet-q state is a complicated non-coplanar state which is mostly composed of equal amounts of the six $\{\frac{3}{4}\frac{3}{4}0\}$ wavevectors. Because of the complexity of this state, in this section we only present the results of analysis on a numerical spin configuration generated by an Iterative Minimization simulation with the parameter values $J_1 = -1$, $J_2 = 0.1$ on a lattice of size $4 \times 4 \times 4$ with periodic boundary conditions.

In this state, it turns out that the site energy \mathcal{E}_i of the spins takes on only six different values: thus we can organize the spins by site energy into six sublattices in real space, each of which has the periodicity of a $2 \times 2 \times 2$ supercell (and is not itself a Bravais lattice). In fact, the sites in each sublattice are equivalent by symmetries of the ground state. The site energy and number of spins in each sublattice is given in table II; the site positions for each sublattice are given in Appendix C.

Sublattices 3 and 4 are the sublattices of highest symmetry in this configuration. They are each made up of tetrahedra of spins. The tetrahedra in sublattice 4 sit on the sites of a body-centered cubic (B.C.C.) lattice with a unit cell of size $2 \times 2 \times 2$. The tetrahedra of spins in sublattice 3 combine with those in sublattice 4 to create a simple cubic lattice of tetrahedra with a unit cell of size $1 \times 1 \times 1$. The spins in sublattice 3 point towards the 12 edge-midpoints of a cube in spin space and the spins in sublattice 4 point towards the eight corners of that same cube.

The nearest neighbors of the spins in sublattices 3 and 4 are distributed throughout the six sublattices. Because sublattices 3 and 4 are made up of tetrahedra, three of the six nearest neighbors of each spin in these two sublattices lie in the same sublattice as that spin. The other three nearest neighbors of the spins in sublattice 4 (there are $192 = 3 \times 64$ of them) are contained in sublattice 5 (these are the only spins in sublattice 5). The other three nearest neighbors of each of the spins in sublattice 3 (there are $576 = 3 \times 192$ of them) are distributed throughout sublattices 1, 2 and 6.

α	A_α	B_α	C_α	D_α	E_α	F_α
1	$-c_1$	c_2	$-c_1$	$-c_2$	c_1	$-c_2$
2	$-c_1$	c_2	c_2	c_1	$-c_2$	c_1
3	c_2	$-c_1$	$-c_1$	$-c_2$	$-c_2$	c_1
4	c_2	$-c_1$	c_2	c_1	c_1	$-c_2$

TABLE III: Coefficients for the approximate parameterization (6.2) of the Kawamura Sextuplet-q state. The greek letter α indexes the four F.C.C. sublattices and the coefficients are all given in terms of the two constants $c_1 \approx 0.73$ and $c_2 \approx 0.27$.

Next we present the results of a least-squares fit of this numerical spin configuration to functions of the form $c_j \sin(\mathbf{q}_j \cdot \mathbf{r} + \phi_j)$ where \mathbf{q}_j is one of the wavevectors of type $\{\frac{3}{4}\frac{3}{4}0\}$ (an optimal L.T. wavevector) and the c_j and ϕ_j are the undetermined fitting parameters. We use the condensed notation

$$\Phi_{xy} = 2\pi \left(\frac{3}{4}x + \frac{3}{4}y \right) \quad (6.1a)$$

$$\bar{\Phi}_{xy} = 2\pi \left(\frac{3}{4}x - \frac{3}{4}y \right), \quad (6.1b)$$

and a similar notation for phase functions involving x and z or involving y and z , to simplify the presentation of this state. Idealizing the results of the least square fit gives an approximate parameterization of this state in each F.C.C. sublattice of the form

$$\begin{aligned} \mathbf{S}_\alpha = & \left\{ A_\alpha \sin \left(\Phi_{yz} - \frac{\pi}{8} \right) + B_\alpha \sin \left(\bar{\Phi}_{yz} \right) \right\} \hat{\mathbf{e}}_1 \\ & + \left\{ C_\alpha \sin \left(\Phi_{xz} + \frac{\pi}{8} \right) + D_\alpha \sin \left(\bar{\Phi}_{xz} + \frac{\pi}{4} \right) \right\} \hat{\mathbf{e}}_2 \\ & + \left\{ E_\alpha \sin \left(\Phi_{xy} + \frac{\pi}{8} \right) + F_\alpha \sin \left(\bar{\Phi}_{xy} + \frac{\pi}{4} \right) \right\} \hat{\mathbf{e}}_3 \end{aligned} \quad (6.2)$$

where the values of the coefficients $A_\alpha, B_\alpha, C_\alpha, D_\alpha, E_\alpha$ and F_α are given for each sublattice in table III.

We can see from (6.2) that if one fixes the x and y coordinates and moves in the z -direction, then the spin configuration looks roughly like a superposition of two distorted conic spirals about the z -axis. A similar statement holds if one fixes the x and z coordinates and moves in the y -direction or fixes the y and z coordinates and moves in the x -direction.

The energy per site for this state is $\bar{\mathcal{E}} = -1.2164$.

B. Anharmonic selection as a consequence of normalization

Although the parameterization (6.2) looks relatively clean, it is not normalized on all of the lattice sites. This is because the Kawamura Sextuplet-q state is not constructed solely from $\{\frac{3}{4}\frac{3}{4}0\}$ wavevectors. A closer look at the Fourier Transform of the numerical spin configuration found in Iterative Minimization simulations shows that it also contains small contributions from wavevectors like $2\pi(\frac{1}{4}, \frac{1}{2}, \frac{3}{4})$, $2\pi(\frac{1}{4}, \frac{1}{2}, -\frac{3}{4})$ and $2\pi(\frac{1}{2}, \frac{1}{4}, -\frac{1}{4})$, even though these are not optimal Luttinger-Tisza wavevectors. The first two of these wavevectors are

equivalent by a symmetry of the F.C.C. lattice (reflection through the x - y plane), so they give the same eigenvalues for the matrix $\tilde{J}(\mathbf{q})$. The third kind of wavevector is not equivalent to the first two.

It turns out that wavevectors of these three types are actually just linear combinations of three of the optimal L.T. wavevectors. For example, we can write $2\pi(\frac{3}{4}, -\frac{3}{4}, 0) + 2\pi(\frac{3}{4}, -\frac{3}{4}, 0) + 2\pi(\frac{3}{4}, 0, \frac{3}{4}) = 2\pi(\frac{9}{4}, -\frac{3}{2}, \frac{3}{4})$. But we may add to this wavevector a reciprocal lattice vector of the form $2\pi(-2, 2, 0)$ to map it back to a wavevector in the first Brillouin zone. We see then that this linear combination of optimal L.T. wavevectors is equivalent to the wavevector $2\pi(\frac{1}{4}, \frac{1}{2}, \frac{3}{4})$. It turns out that the small contributions from these three kinds of wavevectors can be understood by looking at what happens to our approximate parameterization when we normalize it.

To normalize the parameterization (6.2), we would compute

$$\hat{\mathbf{s}}_i = \frac{\mathbf{s}_i}{\sqrt{|\mathbf{s}_i|^2}} \quad (6.3)$$

for every spin. We can rewrite the magnitude of the spin \mathbf{s}_i as $\sqrt{|\mathbf{s}_i|^2} = \sqrt{1 + (|\mathbf{s}_i|^2 - 1)}$. Taylor expanding the reciprocal of this quantity about the point $|\mathbf{s}_i|^2 = 1$ (where the state is normalized), we find

$$\hat{\mathbf{s}}_i = \mathbf{s}_i \left[1 - \frac{1}{2} (|\mathbf{s}_i|^2 - 1) + \dots \right]. \quad (6.4)$$

So the first order correction to the non-unit vector spin \mathbf{s}_i includes a term $|\mathbf{s}_i|^2 \mathbf{s}_i$. It is from this cubic term that we get corrections to the state that involve wavevectors which are a linear combination of three of the optimal Luttinger-Tisza wavevectors (if we wrote out \mathbf{s}_i as an exponential Fourier series, we would see the addition of wavevectors happening in the exponents).

VII. A NEW VARIETY OF DOUBLE-TWIST STATE

In the region $J_1 > 0$, $-.68 \leq J_2 \leq -.43$, we find a state which is chiefly composed of a dominant set of two of the six $\{\frac{3}{4}\frac{3}{4}0\}$ wavevectors and a sub-dominant set of two of the other wavevectors of this type, and these four wavevectors all lie on the points of a cross in reciprocal space. For example, this state might be made from the wavevectors $2\pi(\frac{3}{4}, \frac{3}{4}, 0)$, $2\pi(\frac{3}{4}, -\frac{3}{4}, 0)$, $2\pi(\frac{3}{4}, 0, \frac{3}{4})$ and $2\pi(\frac{3}{4}, 0, -\frac{3}{4})$ with the Fourier amplitudes of the first two wavevectors being approximately 1.40 times the Fourier amplitudes of the second two wavevectors. Luttinger-Tisza analysis confirms that wavevectors of the type $\{\frac{3}{4}\frac{3}{4}0\}$ are the optimal wavevectors for this state.

Although this state is mostly constructed from $\{\frac{3}{4}\frac{3}{4}0\}$ wavevectors, it also contains small contributions from $\{\frac{3}{4}\frac{1}{4}0\}$ wavevectors. These extra wavevectors aid in normalizing this state, since one cannot construct a normalized state from $\{\frac{3}{4}\frac{3}{4}0\}$ wavevectors alone.

This state shares three characteristics in common with the Double-Twist state found on the Octahedral lattice in Ref. 1:

- (1) There is a distinguished direction $\hat{\mathbf{m}}$ in real space and also a distinguished direction $\hat{\mathbf{e}}_3$ in spin space. This state can be written using a basis for spin space that uses the fixed basis vector $\hat{\mathbf{e}}_3$ and two rotating basis vectors $\hat{\mathbf{A}}(\mathbf{r} \cdot \hat{\mathbf{m}})$ and $\hat{\mathbf{B}}(\mathbf{r} \cdot \hat{\mathbf{m}})$ which lie in the plane perpendicular to $\hat{\mathbf{e}}_3$, so that $\hat{\mathbf{A}}(\mathbf{r} \cdot \hat{\mathbf{m}}) \times \hat{\mathbf{B}}(\mathbf{r} \cdot \hat{\mathbf{m}}) = \hat{\mathbf{e}}_3$. As one moves in the $\hat{\mathbf{m}}$ direction in real space the rotating basis vectors $\hat{\mathbf{A}}(\mathbf{r} \cdot \hat{\mathbf{m}})$ and $\hat{\mathbf{B}}(\mathbf{r} \cdot \hat{\mathbf{m}})$ spiral about the fixed vector $\hat{\mathbf{e}}_3$ in spin space.
- (2) There is a second direction $\hat{\mathbf{n}}$ in real space orthogonal to the $\hat{\mathbf{m}}$ direction, with the property that the spins also spiral as one moves in the $\hat{\mathbf{n}}$ direction, although not about the $\hat{\mathbf{e}}_3$ axis in spin space. Since the rotating basis vectors stay put as one moves in the $\hat{\mathbf{n}}$ direction, this second kind of spiral is completely independent from the first kind.
- (3) Both distinct kinds of spiraling behavior are controlled by the same type of wavevector.

To summarize, this state gets its name from the fact that the spins are tracing out two different kinds of spirals in two directions which are perpendicular to each other, but these two spirals are controlled by the same type of wavevector. In the Double-Twist state that we find on the Pyrochlore lattice the distinguished direction $\hat{\mathbf{m}}$ in real space is a $\langle 100 \rangle$ direction, which we take to be the z-direction in our discussion of this state. The second spiraling direction $\hat{\mathbf{n}}$ is then the x- or y-direction. Both kinds of spiral are controlled by a $\{\frac{3}{4}\frac{3}{4}0\}$ wavevector.

We now present an approximate parameterization of this state obtained by performing a least squares fit of a numerical spin configuration found in an Iterative Minimization simulation onto sines and cosines of $\mathbf{q} \cdot \mathbf{r}$, where \mathbf{q} is a $\{\frac{3}{4}\frac{3}{4}0\}$ wavevector (an optimal L.T. wavevector). This simulation was performed with the parameter values $J_1 = 1$ and $J_2 = -0.6$ on a lattice of size $4 \times 4 \times 4$ using periodic boundary conditions.

The two dominant $\{\frac{3}{4}\frac{3}{4}0\}$ wavevectors making up this state are $2\pi(\frac{3}{4}, \frac{3}{4}, 0)$ and $2\pi(\frac{3}{4}, -\frac{3}{4}, 0)$ and the two subdominant wavevectors making up this state are $2\pi(\frac{3}{4}, 0, \frac{3}{4})$ and $2\pi(\frac{3}{4}, 0, -\frac{3}{4})$. As in (6.1) we use the condensed notation

$$\Phi_{xy} = 2\pi \left(\frac{3}{4}x + \frac{3}{4}y \right) \quad (7.1a)$$

$$\bar{\Phi}_{xy} = 2\pi \left(\frac{3}{4}x - \frac{3}{4}y \right) \quad (7.1b)$$

$$\Phi_x = 2\pi \left(\frac{3}{4}x \right) \quad (7.1c)$$

with similar notations for arguments involving y and z. We express this state in terms of the two rotating basis vectors

$$\hat{\mathbf{A}}(z) = \cos(\Phi_z) \hat{\mathbf{e}}_1 + \sin(\Phi_z) \hat{\mathbf{e}}_2 \quad (7.2a)$$

$$\hat{\mathbf{B}}(z) = -\sin(\Phi_z) \hat{\mathbf{e}}_1 + \cos(\Phi_z) \hat{\mathbf{e}}_2, \quad (7.2b)$$

α	A'_α	B'_α	C'_α	D'_α	E_α	F'_α	θ_α	ψ_α
1	d_1	d_2	$-d_1$	d_2	d_3	d_4	5.0°	3.8°
2	d_1	d_2	$-d_1$	d_2	d_4	d_3	31.0°	4.5°
3	d_2	d_1	$-d_2$	d_1	d_4	d_3	17.7°	-7.4°
4	d_2	d_1	$-d_2$	d_1	d_3	d_4	18.4°	17.3°

TABLE IV: Coefficients and phase angles for the approximate parameterization (7.3) of the Double-Twist state. The greek letter α indexes the four F.C.C. sublattices and the coefficients are all given in terms of the four constants $d_1 \approx 0.23$, $d_2 \approx 0.76$, $d_3 \approx 0.26$, $d_4 \approx 0.75$. Analysis of multiple examples of this state seems to indicate that $d_1 \neq d_3$ and $d_2 \neq d_4$, even though their values appear to be very similar.

which have been chosen so that $\hat{\mathbf{A}}(z) \times \hat{\mathbf{B}}(z) = \hat{\mathbf{e}}_3$. The approximate parameterization of this state in each F.C.C. sublattice has the form

$$\begin{aligned} \mathbf{S}_\alpha = & \{A'_\alpha \sin(\Phi_y + \theta_\alpha) + B'_\alpha \sin(\Phi_y + \psi_\alpha)\} \hat{\mathbf{A}}(z) \\ & + \{C'_\alpha \cos(\Phi_y + \theta_\alpha) + D'_\alpha \cos(\Phi_y + \psi_\alpha)\} \hat{\mathbf{B}}(z) \\ & + \left\{ E'_\alpha \sin\left(\Phi_{xy} + \frac{\pi}{4}\right) + F'_\alpha \sin\left(\bar{\Phi}_{xy} + \frac{\pi}{8}\right) \right\} \hat{\mathbf{e}}_3 \end{aligned} \quad (7.3)$$

where the values of the coefficients A'_α , B'_α , C'_α , D'_α , E'_α and F'_α and the phase angles θ_α and ψ_α for each sublattice are given in table IV.

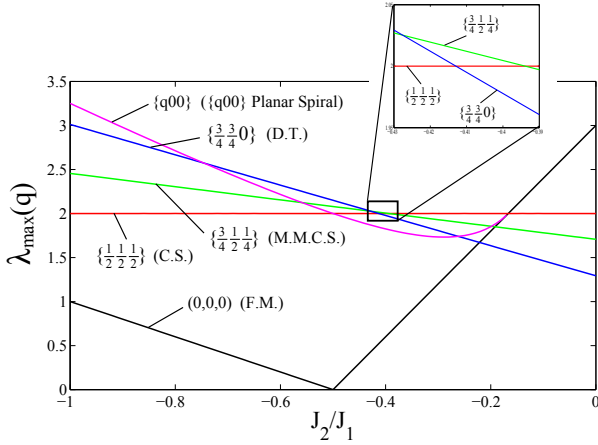
We see from (7.3) that if one holds z constant and moves in the y-direction, the spins spiral (but not about the $\hat{\mathbf{e}}_3$ axis, since the $\hat{\mathbf{e}}_3$ component of the spins changes as one moves in the y-direction), and if one holds y constant and moves in the z-direction the spins spiral about the $\hat{\mathbf{e}}_3$ direction (since the basis vectors $\hat{\mathbf{A}}(z)$ and $\hat{\mathbf{B}}(z)$ change as one moves in the z-direction). In addition, these two spirals are controlled by a $\{\frac{3}{4}00\}$ wavevector. So in this example the $\hat{\mathbf{m}}$ direction is the z-direction and the $\hat{\mathbf{n}}$ direction is the y-direction.

This state has an energy per site $\bar{\mathcal{E}} = -2.2780$.

VIII. MULTIPLY-MODULATED COMMENSURATE SPIRALS

In the small sliver of parameter space $J_1 = 1$, $-0.43 \leq J_2 \leq -0.40$ we find a non-coplanar state with period 4 constructed solely from wavevectors of the types $\{\frac{3}{4}\frac{1}{4}\frac{1}{2}\}$, $\{\frac{3}{4}\frac{3}{4}0\}$ and $\{\frac{1}{4}\frac{1}{4}0\}$ (recall that these three types of wavevector are not equivalent by any symmetry of the F.C.C. lattice). Our prototype of this state uses the four wavevectors $\mathbf{q}_{1+} = 2\pi(\frac{3}{4}, \frac{1}{4}, \frac{1}{2})$, $\mathbf{q}_{1-} = 2\pi(\frac{3}{4}, \frac{1}{4}, -\frac{1}{2})$, $\mathbf{q}_2 = 2\pi(\frac{3}{4}, -\frac{3}{4}, 0)$, and $\mathbf{q}_3 = 2\pi(\frac{1}{4}, -\frac{1}{4}, 0)$, but one can build this state from any set of four wavevectors that is equivalent to these by symmetry. The $\{\frac{3}{4}\frac{1}{4}\frac{1}{2}\}$ wavevectors are the optimal Luttinger-Tisza wavevectors in this region of parameter space. In fact, the largest eigenvalues of the matrix $\bar{\mathbf{J}}(\mathbf{q})$ for these wavevectors at the parameter values $J_1 = 1$, $J_2 = -0.42$ are $\lambda_{max}(\mathbf{q}_{1\pm}) = \lambda_{L.T.} = 2.0195$, $\lambda_{max}(\mathbf{q}_2) = 2.0121$ and $\lambda_{max}(\mathbf{q}_3) = 0.9337$. The Luttinger-Tisza wavevectors $\mathbf{q}_{1\pm}$

FIG. 5: Largest eigenvalue $\lambda_{max}(\mathbf{q})$ of the matrix $\tilde{J}(\mathbf{q})$ vs. J_2/J_1 for the optimal L.T. wavevector of each of the five ground states found in the region $J_1 > 0$, $J_2 < 0$. The name of the corresponding ground state is shown in parentheses next to the label for the type of wavevector. The five ground states are the Ferromagnetic (F.M.), Cuboctahedral Stack (C.S.), Multiply-Modulated Commensurate Spiral (M.M.C.S.), Double-Twist (D.T.) and $\{q00\}$ Planar Spiral states (with wavenumber q for the Planar Spiral given by equation (4.14)). The inset shows the small region $-0.43 \leq J_2/J_1 \leq -0.40$ where the largest eigenvalue for the dominant wavevector in the Multiply-Modulated Commensurate Spiral state briefly crosses above the largest eigenvalue for the wavevectors characterizing the Cuboctahedral Stack and Double-Twist states, confirming that there is a distinct ground state in this small region of the J_1 - J_2 phase diagram.



are the dominant wavevectors in this state, but the state also contains sizable contributions from modes containing the sub-optimal wavevectors \mathbf{q}_2 and \mathbf{q}_3 (see equations (8.5) and (8.6)). So this state is another example of a non-coplanar state which is constructed using an optimal L.T. wavevector and a set of wavevectors which are suboptimal.

Figure 5 shows the largest eigenvalue $\lambda_{max}(\mathbf{q})$ of the matrix $\tilde{J}(\mathbf{q})$ for the optimal Luttinger-Tisza wavevector of each of the five states found in the region $J_1 > 0$, $J_2 < 0$ as a function of J_2/J_1 . It also shows a zoomed in view of the region $-0.43 \leq J_2/J_1 \leq -0.40$ where the largest eigenvalue for wavevectors of the type $\{\frac{3}{4}, \frac{1}{2}, \frac{1}{2}\}$, the main type of wavevector in the Multiply-Modulated Commensurate Spiral state, briefly crosses above the largest eigenvalue of $\tilde{J}(\mathbf{q})$ for the wavevectors used in the Cuboctahedral Stack and Double-Twist states. The fact that the L.T. phase diagram shows a sliver in which $\{\frac{3}{4}, \frac{1}{2}, \frac{1}{2}\}$ wavevectors are optimal is strong evidence that the corresponding spin state found in Iterative Minimization simulations is not merely an artifact of relaxation.

We call this state a Multiply-Modulated Commensurate Spiral (M.M.C.S.) because the spins in this state are tracing out two different spirals in two orthogonal directions and these two spirals are controlled by two different kinds of wavevectors.

In this state there is a distinguished direction $\hat{\mathbf{m}}$ in real space and a distinguished direction $\hat{\mathbf{e}}_3$ in spin space. The distinguished direction in real space is parallel to $\mathbf{q}_{1+} + \mathbf{q}_{1-}$, so $\hat{\mathbf{m}}$ points in the $[310]$ direction in our example state. The spin configuration can be written using a basis in spin space that uses the one fixed basis vector $\hat{\mathbf{e}}_3$ and two rotating basis vectors $\hat{\mathbf{A}}(\xi)$ and $\hat{\mathbf{B}}(\xi)$, where the coordinate $\xi = \mathbf{r} \cdot \hat{\mathbf{m}}$. These two basis vectors lie in the plane perpendicular to $\hat{\mathbf{e}}_3$ and satisfy $\hat{\mathbf{A}}(\xi) \times \hat{\mathbf{B}}(\xi) = \hat{\mathbf{e}}_3$. As one moves in the $\hat{\mathbf{m}}$ direction in real space these two basis vectors rotate counter-clockwise about $\hat{\mathbf{e}}_3$ in spin space. To write this state in the most concise way we also use a second set of two rotating basis vectors $\hat{\mathbf{A}}'(\xi)$ and $\hat{\mathbf{B}}'(\xi)$ lying in the plane perpendicular to $\hat{\mathbf{e}}_3$ and also satisfying $\hat{\mathbf{A}}'(\xi) \times \hat{\mathbf{B}}'(\xi) = \hat{\mathbf{e}}_3$, but this second set rotates clockwise about $\hat{\mathbf{e}}_3$ as one moves in the $\hat{\mathbf{m}}$ direction in real space.

There is also a second distinguished direction $\hat{\mathbf{n}}$ in real space which is parallel to $\mathbf{q}_{1+} - \mathbf{q}_{1-}$, so $\hat{\mathbf{n}}$ points in the $[001]$ direction in our example state. Because \mathbf{q}_{1+} and \mathbf{q}_{1-} differ only in the sign of one component, we have $\hat{\mathbf{m}} \cdot \hat{\mathbf{n}} = 0$. In this state the spins also spiral about the $\hat{\mathbf{e}}_3$ direction in spin space when one moves in the $\hat{\mathbf{n}}$ direction in real space, even though the four basis vectors $\hat{\mathbf{A}}(\xi)$, $\hat{\mathbf{B}}(\xi)$, $\hat{\mathbf{A}}'(\xi)$ and $\hat{\mathbf{B}}'(\xi)$ stay put as one moves in this direction in real space. Finally, the wavevectors that control the spiraling in the $\hat{\mathbf{m}}$ and $\hat{\mathbf{n}}$ directions are not equivalent by symmetry, so the spiraling behavior in this state is different from the spiraling behavior of the Double-Twist state of section VII (the two kinds of spirals in the Double-Twist state are controlled by the same type of wavevector).

Using a diagnostic which counts the number of different spin directions present in a certain state (two spins \mathbf{s}_i and \mathbf{s}_j are considered to point in different directions if $\mathbf{s}_i \cdot \mathbf{s}_j < .99$), we find that the spins in this state point in 42 different directions. The spins in two of the F.C.C. sublattices point in the same 10 directions and the spins in the other two F.C.C. sublattices point in 32 directions which are distinct from the first 10.

Here we present an approximate parameterization of this state which was constructed by idealizing the result of a least square fit of a numerical spin configuration to sines and cosines of $\mathbf{q} \cdot \mathbf{r}$, where \mathbf{q} is a $\{\frac{3}{4}, \frac{1}{2}, \frac{1}{2}\}$, $\{\frac{3}{4}, \frac{3}{4}, 0\}$, or a $\{\frac{1}{4}, \frac{1}{4}, 0\}$ wavevector. This numerical spin configuration was generated by an Iterative Minimization simulation with the parameter values $J_1 = 1$ and $J_2 = -0.43$ on a lattice of size $4 \times 4 \times 4$ using periodic boundary conditions.

The approximate parameterization uses the four wavevectors \mathbf{q}_{1+} , \mathbf{q}_{1-} , \mathbf{q}_2 , and \mathbf{q}_3 defined in the first paragraph of this section. We again use the condensed notation

$$\Phi_{xy} = 2\pi \left(\frac{3}{4}x + \frac{1}{4}y - \frac{1}{16} \right) \quad (8.1)$$

$$\Theta_{xy} = 2\pi \left(\frac{3}{4}x - \frac{3}{4}y - \frac{1}{16} \right) \quad (8.2)$$

$$\Psi_{xy} = 2\pi \left(\frac{1}{4}x - \frac{1}{4}y - \frac{3}{16} \right) \quad (8.3)$$

as a shorthand for these position dependent phase angles. The most concise presentation of this state uses two sets of two rotating basis vectors, all lying in the plane in spin space per-

pendicular to $\hat{\mathbf{e}}_3$. We can write these four basis vectors as

$$\hat{\mathbf{A}}(x, y) = \cos \Phi_{xy} \hat{\mathbf{e}}_1 + \sin \Phi_{xy} \hat{\mathbf{e}}_2 \quad (8.4a)$$

$$\hat{\mathbf{B}}(x, y) = -\sin \Phi_{xy} \hat{\mathbf{e}}_1 + \cos \Phi_{xy} \hat{\mathbf{e}}_2 \quad (8.4b)$$

$$\hat{\mathbf{A}}'(x, y) = \cos \Phi_{xy} \hat{\mathbf{e}}_1 - \sin \Phi_{xy} \hat{\mathbf{e}}_2 \quad (8.4c)$$

$$\hat{\mathbf{B}}'(x, y) = \sin \Phi_{xy} \hat{\mathbf{e}}_1 + \cos \Phi_{xy} \hat{\mathbf{e}}_2 \quad (8.4d)$$

where we have arranged it so that $\hat{\mathbf{A}}(x, y) \times \hat{\mathbf{B}}(x, y) = \hat{\mathbf{A}}'(x, y) \times \hat{\mathbf{B}}'(x, y) = \hat{\mathbf{A}}_0 \times \hat{\mathbf{B}}_0 = \hat{\mathbf{e}}_3$. $\hat{\mathbf{A}}'(x, y)$ is the reflection of $\hat{\mathbf{A}}(x, y)$ over the $\hat{\mathbf{e}}_1$ axis and $\hat{\mathbf{B}}'(x, y)$ is the reflection of $\hat{\mathbf{B}}(x, y)$ over the $\hat{\mathbf{e}}_2$ axis. This parameterization takes quite different forms in the different F.C.C. sublattices. In sublattices 0 and 3, we have

$$\begin{aligned} \mathbf{S}_{\alpha=0,3} = & l_1 \left\{ \sin(\pi z) \hat{\mathbf{A}}'(x, y) \mp \cos(\pi z) \hat{\mathbf{B}}'(x, y) \right\} \\ & + l_2 \left\{ \pm \sin(\pi z) \hat{\mathbf{A}}(x, y) - \cos(\pi z) \hat{\mathbf{B}}(x, y) \right\} \\ & + \{ l_3 \sin \Theta_{xy} + l_4 \sin \Psi_{xy} \} \hat{\mathbf{e}}_3, \end{aligned} \quad (8.5)$$

where the top (bottom) sign in the plus/minus and minus/plus signs corresponds to the zeroth (third) F.C.C. sublattice and the coefficients are $l_1 \approx 0.868$, $l_2 \approx 0.054$, $l_3 \approx 0.699$ and $l_4 \approx 0.076$. These are the two sublattices in which the spins point in 32 different directions, as discussed above. In sublattices 1 and 2, the spin configuration has the same form,

$$\begin{aligned} \mathbf{S}_{\alpha=1,2} = & 2l_3 \cos(\pi z) \hat{\mathbf{B}}'(x, y) \\ & + \{ l_5 \sin \Theta_{xy} + l_6 \sin \Psi_{xy} \} \hat{\mathbf{e}}_3, \end{aligned} \quad (8.6)$$

where $l_5 \approx 0.228$, $l_6 \approx 0.011$ and l_3 is the same coefficient that appeared in (8.5). These are the two sublattices in which the spins point in the same 10 directions.

In this parameterization $\hat{\mathbf{m}}$ points in the $[310]$ direction and $\hat{\mathbf{n}}$ points in the $[001]$ direction. Furthermore, the spiraling in the $\hat{\mathbf{m}}$ direction is controlled by the wavevector $2\pi(\frac{3}{4}, \frac{1}{4}, 0)$ and the spiraling in the $\hat{\mathbf{n}}$ direction is controlled by the wavevector $2\pi(0, 0, \frac{1}{2})$, and these two wavevectors are clearly not of the same type.

The energy per site for this state is $\bar{\mathcal{E}} = -2.0131$.

IX. CONCLUSION

In conclusion, we have surveyed the full range of the phase diagram of classical ground states with nearest and second-nearest neighbor exchange couplings in the Pyrochlore lattice (Figure 2 and Table I). Large swathes of the phase diagram (roughly those in which $|J_2| > |J_1|$) are dominated by the ferromagnet or a relatively simple coplanar spiral phase, but with smaller $|J_2|$ values (for either sign of J_1), a zoo of complex non-coplanar phases were found.

In a similar study of the Octahedral lattice, which formed the model for this one, three categories of non-coplanar state were identified, with only one or two examples of each on the Octahedral lattice, and our results on the Pyrochlore fit into the same categories. One generic category is an ideal

Luttinger-Tisza state, in which three degenerate ordering vectors are matched with three spin directions to form a highly symmetric, already normalized state with no admixture of other modes needed. On the Octahedral lattice these were the two cuboctahedral states; our sole example on the Pyrochlore is also cuboctahedral (Sec. V). The second category was multiple-wavevector commensurate states, dominated by a star of symmetry-related wavevectors but admixing others. On the Octahedral lattice, the only example was the “double-twist”; on the Pyrochlore, we have found *three* representatives: the Kawamura states (Sec. VI), a kind of Double-Twist state (Sec. VII), and a “Multiply-Modulated Commensurate Spiral” (M.M.C.S.) state (Sec. VIII). The third category was “conic spirals” which were stackings of layers with a uniform spin direction in each layer, which are built from two unrelated but nearly degenerate spin modes, one of them being generically incommensurate. Being layered, these states can be optimized after projecting all interactions onto a one-dimensional “chain lattice” [1], as we outlined in Sec. II E. A corollary is that if a non-coplanar state is forced, the layers must be inequivalent, which is indeed the case for the (111) layering in which we did find a conic spiral state (Appendix B) in the Pyrochlore lattice. In both the Octahedral lattice and now in the Pyrochlore lattice, it was difficult to stabilize a conic spiral using the first few neighbor couplings: in the Pyrochlore J_3 and J'_3 were needed.

When we examine the whole phase diagram, there seems to be a rough tendency that the wavevectors used for the (J_1, J_2) ground state are the same as those used for $(-J_1, -J_2)$; for example, the Double-Twist state is diametrically opposite the Kawamura state in Figure 2 and both use optimal wavevectors of type $\{\frac{3}{4}, \frac{3}{4}, 0\}$; the $\mathbf{q} = \mathbf{0}$ antiferromagnet is opposite the ferromagnet which is (of course) also a $\mathbf{q} = \mathbf{0}$ state. There is a plausible reason for this trend. Notice first that the matrix of J_{ij} ’s (in real space) has no diagonal terms, so its trace must be zero. The same must be true for its Fourier transform, so the sum of the four eigenvalues of $\tilde{J}(\mathbf{q})$ is zero at every wavevector. The optimum wavevector $\mathbf{Q}_{L.T.}$ occurs at the point in the zone where one branch of the eigenvalue spectrum has its greatest positive excursion. Necessarily, the *sum* of the other three eigenvalues must have its greatest *negative* excursion at the same wavevector: not uncommonly, that will be the point of the single most negative excursion. But if we reverse the signs of all couplings, the L.T. matrix is the same except for a global sign, and the greatest negative excursion becomes the greatest positive one, i.e. the optimal mode.

Acknowledgments

We thank R. Z. Lamberty for discussions and advice regarding the numerical aspects of this project. This work was supported by NSF grant DMR-1005466.

Appendix A: Fourier Transform of the Interactions for the Pyrochlore Lattice

In this appendix we present the matrix $\tilde{J}(\mathbf{q})$ for the Pyrochlore lattice including interactions J_1 , J_2 , J_3 and J'_3 (i.e. including both kinds of third nearest neighbor interaction). One can calculate the elements of this matrix using equation

(2.7). The matrix is:

$$\tilde{J}(\mathbf{q}) = J_1 \underline{\mathbf{M}}_2 + J_2 \underline{\mathbf{M}}_2 + J_3 \underline{\mathbf{M}}_3 + J'_3 \underline{\mathbf{M}}'_3 \quad (\text{A1})$$

where

$$\underline{\mathbf{M}}_1 = \begin{pmatrix} 0 & \cos(\frac{q_y+q_z}{4}) & \cos(\frac{q_x+q_z}{4}) & \cos(\frac{q_x+q_y}{4}) \\ \cos(\frac{q_y+q_z}{4}) & 0 & \cos(\frac{q_x-q_y}{4}) & \cos(\frac{q_x-q_z}{4}) \\ \cos(\frac{q_x+q_z}{4}) & \cos(\frac{q_x-q_y}{4}) & 0 & \cos(\frac{q_y-q_z}{4}) \\ \cos(\frac{q_x+q_y}{4}) & \cos(\frac{q_x-q_z}{4}) & \cos(\frac{q_y-q_z}{4}) & 0 \end{pmatrix} \quad (\text{A2})$$

$$\underline{\mathbf{M}}_2 = 2 \begin{pmatrix} 0 & \cos(\frac{q_x}{2}) \cos(\frac{q_y-q_z}{4}) & \cos(\frac{q_y}{2}) \cos(\frac{q_z-q_x}{4}) & \cos(\frac{q_z}{2}) \cos(\frac{q_x-q_y}{4}) \\ \cos(\frac{q_x}{2}) \cos(\frac{q_y-q_z}{4}) & 0 & \cos(\frac{q_z}{2}) \cos(\frac{q_x+q_y}{4}) & \cos(\frac{q_y}{2}) \cos(\frac{q_x+q_z}{4}) \\ \cos(\frac{q_y}{2}) \cos(\frac{q_z-q_x}{4}) & \cos(\frac{q_z}{2}) \cos(\frac{q_x+q_y}{4}) & 0 & \cos(\frac{q_x}{2}) \cos(\frac{q_y+q_z}{4}) \\ \cos(\frac{q_z}{2}) \cos(\frac{q_x-q_y}{4}) & \cos(\frac{q_y}{2}) \cos(\frac{q_x+q_z}{4}) & \cos(\frac{q_x}{2}) \cos(\frac{q_y+q_z}{4}) & 0 \end{pmatrix} \quad (\text{A3})$$

To concisely express the matrices that go with the two kinds of third nearest neighbor interaction, we introduce the condensed notation

$$C_{xy} = \cos\left(\frac{q_x + q_y}{2}\right) \quad (\text{A4a})$$

$$\bar{C}_{xy} = \cos\left(\frac{q_x - q_y}{2}\right) \quad (\text{A4b})$$

and a similar notation for cosine terms with arguments using q_y and q_z .

$$\underline{\mathbf{M}}_3 = \begin{pmatrix} C_{xy} + C_{xz} + C_{yz} & 0 & 0 & 0 \\ 0 & \bar{C}_{xy} + \bar{C}_{xz} + \bar{C}_{yz} & 0 & 0 \\ 0 & 0 & \bar{C}_{xy} + C_{xz} + \bar{C}_{yz} & 0 \\ 0 & 0 & 0 & C_{xy} + \bar{C}_{xz} + \bar{C}_{yz} \end{pmatrix} \quad (\text{A5})$$

$$\underline{\mathbf{M}}'_3 = \begin{pmatrix} \bar{C}_{xy} + \bar{C}_{xz} + \bar{C}_{yz} & 0 & 0 & 0 \\ 0 & C_{xy} + C_{xz} + \bar{C}_{yz} & 0 & 0 \\ 0 & 0 & C_{xy} + \bar{C}_{xz} + C_{yz} & 0 \\ 0 & 0 & 0 & \bar{C}_{xy} + C_{xz} + C_{yz} \end{pmatrix} \quad (\text{A6})$$

There are a few interesting things about this matrix. While $\tilde{J}(\mathbf{q})$ is generally a hermitian matrix, it is symmetric in our case because every site on the Pyrochlore lattice is a center of inversion symmetry. Secondly, only J_3 and J'_3 terms appear on the diagonals since these are the only interactions that act between spins in the same F.C.C. sublattice. The J_1 and J_2 interactions only act between sites in different F.C.C. sublattices, so these show up only in off-diagonal terms.

Appendix B: A New Kind of Alternating Conic Spiral State

Although no conic spiral-type ground states are found in the J_1 - J_2 phase diagram of (2.1), conic spiral ground states can

be stabilized on the Pyrochlore lattice for certain sets of interactions. With the interactions $J_1 > 0$, $J_3 > 0$ and $J'_3 < 0$, we find a new type of Alternating Conic Spiral state when the magnitude of J'_3 is much larger than the magnitudes of J_1 and J_3 . Our state is distinct from the Alternating Conic Spiral found in Ref. 1 because the wavevector which controls the spiraling behavior is not parallel to the wavevector which controls the alternating behavior. This means that the component of the spins perpendicular to the conic axis spiral about that axis when you move in one direction in the lattice, and the component of the spins parallel to the conic axis alternates in sign when you move in a completely different direction in the lattice.

This state is made up of two different wavevectors, \mathbf{q}_1 and \mathbf{q}_2 . The first wavevector \mathbf{q}_1 controls the spiraling behavior and it is likely that \mathbf{q}_1 does not have to be commensurate with the lattice (as is the case for the spiraling wavevector in the $\{q00\}$ planar spiral of section IV E). The second wavevector \mathbf{q}_2 controls the alternating behavior and in order for this state to be normalized it must be commensurate with the lattice and satisfy $\cos(\mathbf{q}_2 \cdot \mathbf{r}) = \pm 1$ on all lattice sites \mathbf{r} . As mentioned above, \mathbf{q}_1 and \mathbf{q}_2 are not parallel.

We can express this state most concisely using one rotating basis vector. If we define the phase $\Phi = \mathbf{q}_1 \cdot \mathbf{r}$, then we can write this basis vector as

$$\hat{\mathbf{A}}(\mathbf{r}) = \cos(\Phi)\hat{\mathbf{e}}_1 + \sin(\Phi)\hat{\mathbf{e}}_2. \quad (\text{B1})$$

With this rotating basis vector the parameterization of this state takes the form

$$\mathbf{s}_0 = \sin \alpha \hat{\mathbf{A}}(\mathbf{r}) + \cos \alpha \cos(\mathbf{q}_2 \cdot \mathbf{r}) \hat{\mathbf{e}}_3 \quad (\text{B2a})$$

$$\mathbf{s}_1 = \hat{\mathbf{A}}(\mathbf{r}) \quad (\text{B2b})$$

$$\mathbf{s}_2 = \sin \alpha \hat{\mathbf{A}}(\mathbf{r}) + \cos \alpha \cos(\mathbf{q}_2 \cdot \mathbf{r}) \hat{\mathbf{e}}_3 \quad (\text{B2c})$$

$$\mathbf{s}_3 = \cos(\mathbf{q}_2 \cdot \mathbf{r}) \hat{\mathbf{e}}_3. \quad (\text{B2d})$$

We can see from (B2) that the spins in F.C.C. sublattices 0 and 2 are performing Alternating Conic Spirals, the spins in F.C.C. sublattice 1 are performing a planar spiral about the conic axis, and the spins in F.C.C. sublattice 3 are alternating pointing parallel and antiparallel to the axis of the conic spiral.

An Iterative Minimization simulation at the parameter values $J_1 = 1$, $J_3 = 1$ and $J'_3 = -4$ on a lattice of size $4 \times 4 \times 4$ with periodic boundary conditions found this new kind of Alternating Conic Spiral with $\mathbf{q}_1 = 2\pi(-\frac{3}{4}, -\frac{1}{2}, \frac{1}{4})$, $\mathbf{q}_2 = 2\pi(-\frac{1}{2}, \frac{1}{2}, \frac{1}{2})$ and cone angle $\alpha \approx 0.92$ (radians). As J'_3 is varied in this region, Fourier Transforms of the numerical spin configurations found in Iterative Minimization simulations still show large peaks near $\{\frac{1}{2}\frac{1}{2}\frac{1}{2}\}$ type wavevectors. For this reason, we suspect that the vector \mathbf{q}_2 is always a $\{\frac{1}{2}\frac{1}{2}\frac{1}{2}\}$ type wavevector (and therefore commensurate with the lattice). On the other hand, it appears that \mathbf{q}_1 and the cone angle α can vary continuously.

For this set of parameter values, the optimal Luttinger-Tisza wavevector is of the type $\{\frac{1}{2}\frac{1}{2}\frac{1}{2}\}$, so \mathbf{q}_2 is equal to $\mathbf{Q}_{L.T.}$. The Luttinger-Tisza eigenvalue is $\lambda_{L.T.} = 7$. We find, however, that $\lambda_{max}(\mathbf{q}_1) = 6.8629$, which is only slightly less than 7. So this is another example of a non-coplanar state which is

composed of an optimal L.T. wavevector, \mathbf{q}_2 , and a second type of wavevector, \mathbf{q}_1 , which is only slightly sub-optimal. This provides further evidence for the hypothesis advanced in Ref. 1 that many non-coplanar states are made from combinations of optimal Luttinger-Tisza wavevectors and wavevectors that are only slightly suboptimal.

Appendix C: Unit cells of the six sublattices of the Kawamura Sextuplet-q State

These are the locations of lattice sites in the $2 \times 2 \times 2$ unit cells of the six sublattices for the example of the Kawamura Sextuplet-q state example presented above (section VI A). This spin configuration was generated from an Iterative Minimization simulation with parameter values $J_1 = -1$, $J_2 = 0.1$ on a lattice of size $4 \times 4 \times 4$.

1. F.C.C.0: (0,0,0), (1,1,1), (.5,0,1.5), (1.5,1,.5), (.5,1.5,0), (1.5,.5,1)
 F.C.C.1: (.5,1.25,.75), (1.5,.25,1.75), (0,.75,.75), (1,1.75,1.75), (.5,.75,1.25), (1.5,1.75,.25)
 F.C.C.2: (.25,1,.25), (1.25,0,1.25), (.75,1,1.75), (1.75,0,.75), (.25,.5,1.75), (1.25,1.5,.75)
 F.C.C.3: (.25,.25,1), (1.25,1.25,0), (.25,1.75,.5), (1.25,.75,1.5), (.75,1.75,1), (1.75,.75,0)
2. F.C.C.0: (0,1,0), (1,1,0), (1.5,0,.5), (1.5,0,1.5), (.5,.5,1), (5,1.5,1)
 F.C.C.1: (.5,.25,1.75), (.5,1.25,1.75), (0,1.75,.75), (1,1.75,.75), (1.5,.75,.25), (1.5,.75,1.25)
 F.C.C.2: (.25,0,.25), (.25,0,1.25), (.75,1,.75), (1.75,1,.75), (1.25,.5,1.75), (1.25,1.5,1.75)
 F.C.C.3: (1.25,.25,1), (1.25,1.25,1), (.25,.75,.5), (.25,.75,1.5), (.75,1.75,0), (1.75,1.75,0)
3. F.C.C.0: (0,.5,.5), (0,.5,1.5), (0,1.5,.5), (1,.5,1.5), (1,1.5,.5), (1,1.5,1.5)
 F.C.C.1: (0,.25,.25), (0,.25,1.25), (0,1.25,.25), (1,.25,1.25), (1,1.25,.25), (1,1.25,1.25)
 F.C.C.2: (.75,.5,1.25), (.75,1.5,.25), (.75,1.5,1.25), (1.75,.5,.25), (1.75,.5,1.25), (1.75,1.5,.25)
 F.C.C.3: (.75,.25,1.5), (.75,1.25,.5), (.75,1.25,1.5), (1.75,.25,.5), (1.75,.25,1.5), (1.75,1.25,.5)
4. F.C.C.0: (0,1.5,1.5), (1,.5,.5)
 F.C.C.1: (0,1.25,1.25), (1,.25,.25)
 F.C.C.2: (.75,.5,.25), (1.75,1.5,1.25)
 F.C.C.3: (.75,.25,.5), (1.75,1.25,1.5)
5. F.C.C.0: ((0,1,1), (1,0,0), (.5,0,.5), (1.5,1,1.5), (.5,.5,0), (1.5,1.5,1)
 F.C.C.1: (.5,.25,.75), (1.5,1.25,1.75), (0,1.75,1.75), (1,.75,.75), (.5,.75,.25), (1.5,1.75,1.25)
 F.C.C.2: (.25,1,1.25), (1.25,0,.25), (.75,0,.75), (1.75,1,1.75), (.25,1.5,1.75), (1.25,.5,.75)
 F.C.C.3: (.25,1.25,1), (1.25,.25,0), (.25,1.75,1.5), (1.25,.75,.5), (.75,.75,0), (1.75,1.75,1)

6. F.C.C.0: (0,0,1), (1,0,1), (.5,1.5), (.5,1,1.5), (1.5,.5,0),
 (1.5,1.5,0)
 F.C.C.1: (1.5,.25,.75), (1.5,1.25,.75), (0,.75,1.75),
 (1,.75,1.75), (.5,1.75,.25), (.5,1.75,1.25)
 F.C.C.2: (1.25,1,.25), (1.25,1,1.25), (.75,0,1.75),

(1.75,0,1.75), (.25,.5,.75), (.25,1.5,.75)
 F.C.C.3: (.25,.25,0), (.25,1.25,0), (1.25,1.75,.5),
 (1.25,1.75,1.5), (.75,.75,1), (1.75,.75,1)

-
- [1] S. Sklan and C. L. Henley, preprint (arXiv:1209.1381) “Non-planar ground states of frustrated antiferromagnets on an octahedral lattice”.
- [2] A. P. Ramirez, M.R.S. Bulletin, Volume 30, June 2005.
- [3] T. A. Kaplan and N. Menyuk, Phil. Mag. 87, 3711 (2006).
- [4] C. L. Henley, Phys. Rev. Lett. 62, 2056 (1989).
- [5] C. L. Henley, Ann. Phys. (N. Y.) 156, 368-411 (1984),
- [6] J. M. Luttinger and L. Tisza, Phys. Rev. 70, 954 (1946).
- [7] D. H. Lyons and T. A. Kaplan, J. Phys. Chem. Solids, 25, 645 (1964).
- [8] G.-W. Chern, R. Moessner, and O. Tchernyshyov Phys. Rev. B 78, 144418 (2008).
- [9] T. Okubo, T. H. Nguyen, and H. Kawamura. Phys. Rev. B 84, 144432 (2011).
- [10] M. Matsuda, J.-H. Chung, S. Park, T. J. Sato, K. Matsuno, H. Aruga-Katori, H. Takagi, K. Kakurai, K. Kamazawa, Y. Tsunoda, I. Kagomiya, C. L. Henley, and S.-H. Lee, Europhys. Lett. 82, 37006 (2008).
- [11] Y. Taguchi, Y. Oohara, H. Yoshizawa, N. Nagaosa, and Y. Tokura, Science 291, 2573 (2001),
- [12] A. Kalitsov, B. Canals, and C. Lacroix, J. Phys. Conf. proc. 145, 012020 (2009).
- [13] M. Taillefumier, B. Canals, C. Lacroix, V. K. Dugaev, and P. Bruno, Phys. Rev. B 74, 085105 (2006)
- [14] N. Nagaosa, J. Sinova, S. Onoda, A. H. MacDonald, and N. P. Ong, Rev. Mod. Phys. 82, 1539 (2010)
- [15] S.-W. Cheong and M. Mostovoy, Nature Materials 8, 13 (2007).
- [16] T. Kimura, Ann. Rev. Mater. Sci. 37, 387 (2007).
- [17] T. Kimura, J. C. Lashley, and A. P. Ramirez, Phys. Rev. B 73, 220401 (2006)
- [18] D. Khomskii, Physics 2, 20 (2009).
- [19] Y. J. Choi, J. Okamoto, D. J. Huang, et al. K. S. Chao, H. J. Lin, C. T. Chen, M. van Veenendaal, T. A. Kaplan, and S. W. Cheong Phys. Rev. Lett. 102, 067601 (2009).
- [20] R. Moessner and J. T. Chalker, Phys. Rev. Lett. 80, 2929 (1998); Phys. Rev. B 58, 12049 (1998).
- [21] D. H. Lyons and T. A. Kaplan, Phys. Rev. 120, 1580 (1960).
- [22] J. Samuel Smart, *Effective field theories of magnetism* (W. B. Saunders, Philadelphia, 1966); see chapter 8.
- [23] E. Rastelli, A. Tassi, and L. Reatto, Physical B & C 97, 1 (1979); E. Rastelli and A. Tassi, J. Phys. C: 19, L423 (1986).
- [24] J. N. Reimers, A. J. Berlinsky, and A. C. Shi, Phys. Rev. B 43, 865 (1991).
- [25] J.-C. Domenge, P. Sindzingre, C. Lhuillier, and L. Pierre, Phys. Rev. B 72, 024433 (2005).
- [26] J.-C. Domenge, C. Lhuillier, L. Messio, L. Pierre, and P. Viot, Phys. Rev. B 77, 172413 (2008).
- [27] L. Messio, C. Lhuillier, and G. Misguich, Phys. Rev. B 83, 184401 (2011).
- [28] M. J. P. Gingras, “Spin ice”, in *Introduction to Frustrated Magnetism: Materials, Experiments, Theory*, eds. C. Lacroix, P. Mendels, F. Mila. (Springer Series in Solid-State Sciences, 2010).
- [29] S. T. Bramwell, M. J. P. Gingras, and J. N. Reimers, J. Appl. Phys. 75, 5523 (1994).
- [30] M. Elhajal, B. Canals, M. Elhajal, and C. Lacroix, Phys. Rev. B 78, 214431 (2008); G.-W. Chern, unpublished preprint (arXiv:1008.3038)
- [31] O. Tchernyshyov, R. Moessner, and S. L. Sondhi, Phys. Rev. Lett. 88, 067203 (2002).
- [32] O. Tchernyshyov, Phys. Rev. Lett. 93, 157206 (2004)
- [33] G.-W. Chern, C.J. Fennie, and O. Tchernyshyov, Phys. Rev. B 74, 060405(R) (2006);
- [34] D. L. Bergman, R. Shindou, G. A. Fiete, and L. Balents, Phys. Rev. B 74, 134409 (2006);
- [35] J.-H. Chung, M. Matsuda, S.-H. Lee, K. Kakurai, H. Ueda, T. J. Sato, H. Takagi, K.-P. Hong, and S. Park, Phys. Rev. Lett. 95, 247204 (2005).
- [36] D. Tsuneishi, M. Ioki, and H. Kawamura, J. Phys. Condens. Matter 19, 145273 (2007).
- [37] T. Nakamura and D. Hirashima, J. Mag. Mag. Materials 310, 1297 (2007).
- [38] G.-W. Chern, Phys. Rev. Lett. 105, 226403 (2010).
- [39] Ref. 8 found that at even higher temperatures, a collinear state based on the same modes is stabilized.